United States
Department of
Agriculture

Forest Service

Forest Pest
Management

Davis, CA

Field Measurements of Helicopter Rotor Wash in Hover and Forward Flight

FPM 95-7
February 1995

Pesticides used improperly can be injurious to human beings, animals, and plants. Follow the directions and heed all precautions on labels. Store pesticides in original containers under lock and key—out of the reach of children and animals—and away from food and feed.

Apply pesticides so that they do not endanger humans, livestock, crops, beneficial insects, fish, and wildlife. Do not apply pesticides where there is danger of drift when honey bees or other pollinating insects are visiting plants, or in ways that may contaminate water or leave illegal residues.

Avoid prolonged inhalation of pesticide sprays or dusts; wear protective clothing and equipment, if specified on the label.

If your hands become contaminated with a pesticide, do not eat or drink until you have washed. In case a pesticide is swallowed or gets in the eyes, follow the first aid treatment given on the label, and get prompt medical attention. If a pesticide is spilled on your skin or clothing, remove clothing immediately and wash skin thoroughly.

NOTE: Some States have restrictions on the use of certain pesticides. Check your State and local regulations. Also, because registrations of pesticides are under constant review by the U.S Environmental Protection Agency, consult your local forest pathologist, county agriculture agent, or State extension specialist to be sure the intended use is still registered.

FPM 95-7
February 1995

Field Measurements of Helicopter Rotor Wash in Hover and Forward Flight

Prepared by:

Milton E. Teske and
Andrew E. Kaufman

Continuum Dynamics, Inc.
P.O. Box 3073
Princeton, NJ 08543

Contract No. 53-0343-4-00009

Prepared for:

USDA Forest Service
Forest Pest Management
2121C Second Street
Davis, CA 95616
(916)757-8342

John W. Barry
Project Officer

C. D. I. Technical Note No. 94-15

Field Measurements of Helicopter Rotor Wash in Hover and Forward Flight

Prepared by

Milton E. Teske
Andrew E. Kaufman

CONTINUUM DYNAMICS, INC.
P. O. BOX 3073
PRINCETON, NEW JERSEY 08543

Prepared under Contract No. 53-0343-4-00009 for

Charles W. George
USDA FOREST SERVICE INTERMOUNTAIN RESEARCH STATION
P. O. BOX 8089
MISSOULA, MONTANA 59807

Bruce S. Grim
U. S. ARMY JOINT CONTACT POINT
DUGWAY PROVING GROUND
DUGWAY, UTAH 84022

John W. Barry
USDA FOREST SERVICE FOREST PEST MANAGEMENT
2121C SECOND STREET, SUITE 102
DAVIS, CALIFORNIA 95616

February 1995

EXECUTIVE SUMMARY

The USDA Forest Service uses helicopters to spray forests with pesticides, spread water or retardants on forest fires, and, along with the U. S. Army, maintains an interest in the propagation of fire along the ground and the movement of contaminants in the air. The dispersing aircraft generally fly low over their target area in an effort to deliver their payloads with as much precision as possible. Up to now, the effect of a passing helicopter on the local meteorology, particularly near a forest fire, has been understood only from a qualitative standpoint. Because the quantitative data are considered important in understanding fire propagation and the dispersal of pesticides and other contaminants, a cooperative field study was recently conducted to collect such data, with the hope that these data may be used to validate models of helicopter wakes, suggest operational methods for fighting forest fires, and provide insight into the dispersal of dusts, aerosols, and other contaminants in the atmosphere.

During the time periods of 26 July to 29 July and 27 September to 1 October, 1994, 181 passes were made by seven helicopters over a row of six towers instrumented with 32 propeller anemometers. These anemometers measured the induced downwash and sidewash velocities generated by the helicopters in hover or forward flight above the towers. Resulting time histories were examined to recover the magnitude and behavior of the induced velocities, in an effort to infer the potential for the helicopters to promote the sideways spread of fire, pesticides, dusts, aerosols, or other contaminants.

Normalized data average values suggest that a significant induced surface sidewash velocity may result from the passage of a helicopter (depending on the size, weight and flight speed of the helicopter, and its height above the ground -- heavier helicopters generate higher surface velocities), that the peak induced sidewash velocity moves slowly along the ground in a tall gust front, and that the induced sidewash velocity remains important for a long period of time. These results enable the better prediction of the spread of fire, pesticides, dusts, aerosols, or other contaminants.

This cooperative study was sponsored by the USDA Forest Service, State and Private Forestry, Forest Pest Management; USDA Forest Service, Intermountain Research Station, Fire Laboratory; and the U. S. Army.

TABLE OF CONTENTS

1. INTRODUCTION

The USDA Forest Service uses helicopters to spray forests with pesticides, spread water or retardants on forest fires, and, along with the U. S. Army, maintains an interest in the propagation of fire along the ground and the movement of contaminants in the air. These aircraft generally fly low over their target area in an effort to deliver their payloads with as much precision as possible. Up to now, the effect of a passing helicopter on the local meteorology, particularly near a forest fire, has been understood only from a qualitative standpoint. The effect of the induced downwash and sidewash velocities may be significant when investigating the advantages of one helicopter versus another with regard to potential of sideways spread of the released spray material; examining the injurious possibility of the induced velocities actually enhancing the ability of a fire to spread; or analyzing the ability of a helicopter to disperse dusts, aerosols, or other contaminants from a specified location. In the case of forest fire fighting, this hypothesis suggests that large fire-fighting helicopters may create a significant induced sidewash velocity, which actually propels the fire sideways and prevents control.

Traditionally, the helicopter flow field may be thought of as a column of air directly under the rotor blades, this column being pushed downward by the blade rotation. Heavier helicopters (such as a Chinook CH-47) induce significantly higher rotor downwash velocities than do lighter helicopters (such as a Bell 206B). As this column of air nears the surface, it spreads out along the ground, creating a sidewash that itself can be quite strong. Anyone who has been around a helicopter, or paid attention to the effects of helicopter wakes shown in action sequences on television or in motion pictures, should be familiar with the intense winds and flying debris produced. Therefore, the concern for helicopter flyby data, raised by the USDA Forest Service and the U. S. Army, is a valid one, and needs to be explored by a field experiment, and subsequent data interpretation and modeling.

In a series of previous field studies for Program WIND ("Winds in Nonuniform Domains"), and in subsequent studies for the U. S. Army, Continuum Dynamics, Inc. set up anemometer tower grids to record the passage of aircraft wingtip vortices (Williamson, Teske and Geyer 1985; Teske, Bilanin and Geyer 1986; Teske, Kaufman and Curbishley 1988 and 1990). In these experimental studies anemometer tower grids recorded the induced vertical velocity time histories as various aircraft repeatedly traversed normal to the tower grid (some of these flybys were by helicopters). These digitized velocity traces produced an aircraft wake signature that could be used to infer the strength and lateral and vertical motion of the aircraft vortex pairs generating the traces. A generalized algorithm located the trailed vortex pairs in all available data, and then inferred their decay properties in the atmosphere (Teske 1988; Bilanin et al. 1989a; Teske, Bilanin and Barry 1993). This decay effect was quantified as a decay constant for subsequent input into the AGDISP and FSCBG aerial spray application models (Bilanin et al. 1989b; Teske et al. 1993).

In the present application the helicopter downwash and subsequent induced horizontal velocities are the important measurements. Consequently, most of the anemometers were set to record the induced horizontal velocity time histories as the helicopters flew over the tower grid. Data were collected with an analog-to-digital board mounted inside a personal computer. The test procedure is summarized in Section 2 of this report. The algorithm used to reduce the data, and the implications of the study findings, are found in Section 3. Conclusions are offered in Section 4.

2. SUMMARY OF TESTS CONDUCTED

TEST AIRCRAFT

Seven different helicopters were used in the field study, including: a Bell 205H, a Bell 206B, a Blackhawk, a Boeing Vertol BV-107, a Chinook CH-47, a Sikorsky S-61, and a Skycrane. The aircraft were tested under fully loaded and empty conditions, where fully loaded conditions were simulated with a water bucket or a known weight hung from the helicopter. The pertinent aircraft characteristics are the following:

Aircraft	Rotor Radius (m)	RPM	Full / Empty Weight (kN)	
Bell 205H	7.4	324	45.3	32.6
Bell 206B	5.5	324	11.4	8.7
Blackhawk	8.0	260	80.1	57.8
Boeing Vertol BV-107	7.6	264	97.9	62.3
Chinook CH-47	9.1	260	214.4	106.8
Sikorsky S-61	9.4	210	85.7	51.1
Skycrane	11.0	185	160.1	115.6

where the rotor radius is in meters (3.28 feet per m) and the weights are in kilo Newtons (one pound equals 4.448 N). The rotor radius is the main rotor radius for the helicopters with two blades (Boeing Vertol BV-107 and Chinook CH-47).

TEST SITE

All tests were performed over open flat terrain near Yuba City, CA at a site used by the USDA Forest Service for helicopter drop tests. The field was approximately 800 m long (in the north-south direction) by 150 m wide. The terrain was flat to the east and west of the field, with a rice paddy to the west (separated by an elevated dirt road) and a fallow field to the east (separated by small shrubs and growth). The test site was plowed soil. The meteorological station was set up to the east of the field near the north-south centerline.

The six anemometer towers were uniformly spaced 18.3 m apart and centered on the field. The towers were located 9.1 m south of the north-south centerline to avoid interfering with panels used to determine aircraft height and speed from video analysis. The tower and anemometer locations are shown schematically in Figure 1. The centerline of the field was marked with orange traffic cones to provide a reference for the pilot. The data acquisition system was housed in a mobile home located along the centerline of the field and 26.2 m south of the towers. The mobile home was equipped with a generator to provide power for the data acquisition system.

The towers used to mount the anemometers (see Figure 1) were telescoping masts extended to their maximum height of 13.7 m. Anemometers were placed as high as possible to capture the top edge of the surface gust front anticipated by the passage of the

helicopter. The towers were placed in a single line normal to the flight path, yielding a grid span of 91.4 m. The tower to the west was identified as tower 1. A total of 32 anemometers were used for the tests. Twenty-four anemometers were mounted horizontally at heights of 3.0, 6.1, 9.1 and 13.7 m from the ground on each tower to measure the horizontal velocity normal to the flight path. In addition to these horizontal V sensors, U-V-W sensors were mounted on tower 3 at 6.1 m and on tower 4 at 13.7 m. Vertical anemometers were also placed on tower 2 at 6.1 m, tower 3 at 13.7 m, tower 4 at 6.1 m, and tower 5 at 6.1 m above the ground.

ANEMOMETERS

Gill anemometers, manufactured by the R. M. Young Company and on loan to the USDA Forest Service from the Transportation Systems Center of the U. S. Department of Transportation, were used for this study. Four-bladed propellers (19 cm in diameter) were coupled with the DC generators to complete the anemometer and were calibrated at 1800 RPM. The anemometers were mounted on the towers and primarily oriented normal to the aircraft flight path to enable measurement of the sidewash. Additional vertical anemometers were used to characterize the downwash from the aircraft. The anemometers were electrically connected to the data acquisition system with filtering capacitors in accordance with manufacturer's recommendations. The wake velocity signals were sampled and recorded by a digital data acquisition system (personal computer based) during the helicopter flights over the towers. Data collection began at least 30 seconds before passage of the helicopters and continued until all of the anemometers appeared to return to ambient rotation, to enable extraction of the mean winds from the transient velocities caused by the helicopters.

DATA ACQUISITION SYSTEM

The data acquisition system consisted of an IBM portable personal computer with two Data Translation DT2801 analog-to-digital converter boards to sample and digitize 32 channels of analog voltage signals from the anemometers. Sampling was carried out at a rate of 100 samples per sec (each anemometer was sampled every 0.34 sec). The full scale analog voltages ±2.50 volts were converted to the digital representations 0 to 4095, and stored in memory. A maximum of four minutes of data could be sampled continuously (before reaching memory limits) and stored for post-test conversion to engineering units and further analysis. Sampling began before the aircraft flyover and continued after the wake passed through the anemometer grid, to provide U-V-W data to extract the mean wind conditions and the downwash event.

TEST MATRIX

Induced velocity data were collected from the wake of helicopters over a representative range of flight conditions. These data could then be used to infer the ground-level flow field generated by the helicopter passage. Velocity data for most aircraft were obtained under fully loaded and empty conditions (with corrections made for the anticipated loss of weight due to fuel expenditure), at various aircraft heights (from 20.4 m to 123.4 m) and a range of aircraft speeds (from hover to 45.8 m/sec). Helicopter heights and aircraft speeds were recorded by Intermountain Fire Sciences Laboratory personnel (C. W. George, personal communication). The complete matrix is given in Tables 1 through 8 for each field data block.

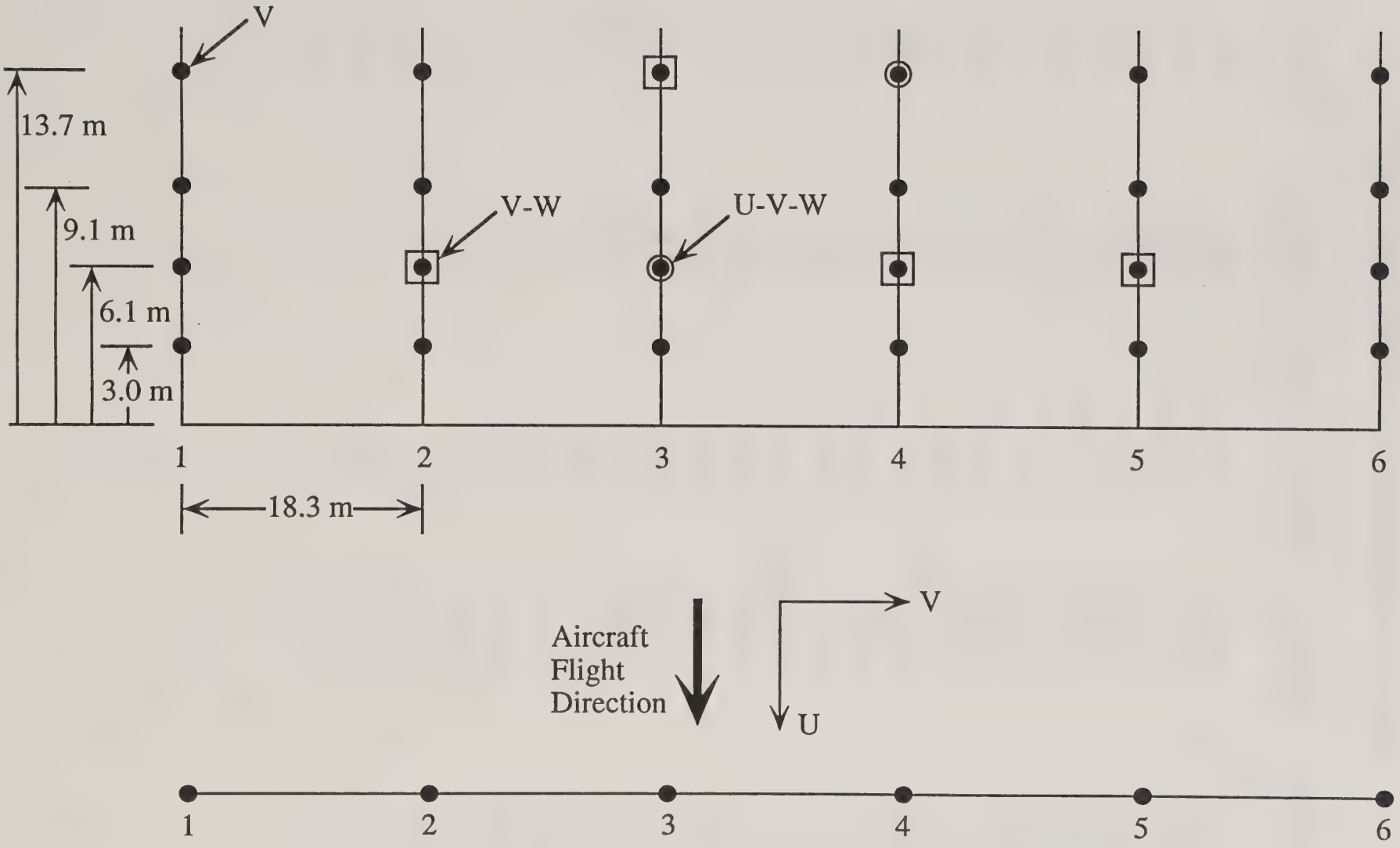

Figure 1. The anemometer tower grid configuration at Yuba City, CA.

Table 1. Test Matrix for the Chinook CH-47 on 26 July 1994.

Run Number	Time	Height (m)	Flight Speed (m/sec)	Weight (kN)
001	10:16 am	82.9	45.3	106.8
002	10:19 am	83.5	35.0	105.8
003	10.23 am	88.4	24.7	104.8
004	10:27 am	93.3	15.9	103.8
005	10:31 am	90.2	Hover	102.8
006	10:35 am	83.8	43.7	101.8
007	10:38 am	85.0	35.0	100.8
008	10:42 am	78.9	23.7	99.8
009	10:46 am	76.2	15.4	98.8
010	10:49 am	61.6	42.7	97.8
011	10:53 am	60.0	34.0	96.8
012	10:57 am	50.6	22.6	95.8
013	11:01 am	44.2	14.4	94.8
014	11:06 am	68.3	Hover	93.8
015	12:13 pm	94.5	45.8	214.4
016	12:17 pm	104.5	36.0	213.4
017	12:21 pm	83.8	24.7	212.4
018	12:25 pm	58.5	14.9	211.4
019	12:28 pm	86.3	45.3	210.4
020	12:30 pm	90.2	35.5	209.4
021	12:34 pm	88.7	25.2	208.4
022	12:37 pm	78.6	15.4	207.4
023	12:41 pm	75.0	Hover	206.4
024	12:45 pm	71.6	Hover	205.4

Table 2. Test Matrix for the Sikorsky S-61 on 27 July 1994.

Run Number	Time	Height (m)	Flight Speed (m/sec)	Weight (kN)
025	7.37 am	90.5	16.5	85.7
026	7:40 am	89.0	14.4	85.5
027	7:47 am	73.5	Hover	85.2
028	7:52 am	79.9	8.2	85.0
029	7:56 am	78.0	9.8	84.7
030	7:59 am	74.7	14.9	84.5
031	8:03 am	58.2	Hover	84.2
032	8:18 am	50.6	5.7	51.1
033	8:21 am	62.5	17.5	50.9
034	8:24 am	48.2	30.9	50.6
035	8:27 am	59.7	42.7	50.4
036	8:34 am	69.2	9.3	50.1
037	8:37 am	75.9	17.0	49.9
038	8:41 am	81.4	Hover	49.6
039	8:44 am	59.1	Hover	49.4
040	8:48 am	38.7	Hover	49.2

Table 3. Test Matrix for the Bell 205H on 28 July 1994.

Run Number	Time	Height (m)	Flight Speed (m/sec)	Weight (kN)
041	8:17 am	25.0	11.8	32.6
042	8:22 am	28.7	20.1	32.4
043	8:25 am	28.3	32.9	32.2
044	8:28 am	27.7	41.7	32.0
045	8:31 am	38.4	14.9	31.7
046	8:34 am	34.7	23.1	31.5
047	8:37 am	36.0	29.8	31.3
048	8:40 am	38.4	39.6	31.1
049	8:43 am	21.9	13.4	30.9
050	8:47 am	21.9	20.1	30.6
051	8:50 am	22.3	29.8	30.4
052	8:52 am	23.5	40.1	30.2
053	8:57 am	21.9	8.2	30.0
054	9:02 am	36.9	Hover	29.7
055	9:07 am	25.3	Hover	29.5
056	9:12 am	20.4	Hover	45.3
057	9:35 am	37.5	11.3	45.0
058	9:38 am	40.2	23.1	44.8
059	9:41 am	34.4	22.1	44.6
060	9:44 am	36.3	29.8	44.4
061	9:47 am	37.2	39.6	44.1
062	9:52 am	35.7	8.7	43.9
063	9:56 am	27.1	8.2	43.7
064	10:00 am	25.6	12.3	43.5
065	10:03 am	27.1	21.1	43.3
066	10:06 am	27.4	30.3	43.0
067	10:09 am	26.8	39.1	42.8
068	10:15 am	25.6	Hover	42.6
069	10:20 am	34.7	Hover	42.4
070	10:46 am	20.4	Hover	41.7

Table 4. Test Matrix for the Bell 206B on 28 July 1994.

Run Number	Time	Height (m)	Flight Speed (m/sec)	Weight (kN)
071	3:30 pm	31.4	11.8	8.7
072	3:33 pm	35.1	13.4	8.6
073	3:37 pm	38.4	19.0	8.6
074	3:40 pm	24.7	7.7	8.6
075	3:42 pm	24.4	10.3	8.6
076	3:45 pm	24.7	13.9	8.5
077	3:47 pm	24.4	26.7	8.5
078	3:50 pm	50.0	6.7	8.5
079	3:53 pm	39.9	11.3	8.5
080	3:56 pm	40.5	17.0	8.5
081	3:59 pm	40.2	Hover	8.4
082	4:03 pm	37.5	Hover	8.4
083	4:07 pm	30.2	Hover	8.4
084	4:11 pm	25.0	Hover	8.4
085	4:29 pm	30.8	7.7	11.4
086	4:31 pm	29.6	9.8	11.4
087	4:34 pm	39.9	6.2	11.4
088	4:37 pm	42.7	7.7	11.4
089	4:41 pm	31.1	Hover	11.3

Table 5. Test Matrix for the Blackhawk on 29 July 1994.

Run Number	Time	Height (m)	Flight Speed (m/sec)	Weight (kN)
090	11:06 am	38.4	11.3	57.8
091	11:10 am	35.7	14.9	57.6
092	11:13 am	32.6	29.3	57.3
093	11:16 am	42.4	40.1	57.1
094	11:22 am	56.4	7.2	56.8
095	11:27 am	50.6	12.9	56.6
096	11:31 am	53.3	15.9	56.3
097	11:34 am	56.4	31.4	56.1
098	11:38 am	63.7	38.1	55.8
099	11:43 am	27.7	6.2	55.6
100	11:47 am	24.7	10.8	55.4
101	11:51 am	24.7	19.5	55.1
102	11:54 am	32.0	31.4	54.9
103	11:58 am	29.9	40.6	54.6
104	12:03 pm	52.1	Hover	54.4
105	12:07 pm	33.2	Hover	54.1
106	12:12 pm	26.8	Hover	53.9

Table 6. Test Matrix for the Boeing Vertol BV-107 on 27 September 1994.

Run Number	Time	Height (m)	Flight Speed (m/sec)	Weight (kN)
107	3:11 pm	51.2	10.8	97.9
108	3:16 pm	67.1	14.4	97.4
109	3:19 pm	60.0	23.7	97.0
110	3:22 pm	55.5	31.9	96.5
111	3:24 pm	57.3	39.6	96.1
112	3:28 pm	78.3	16.5	95.6
113	3:32 pm	76.2	20.1	95.2
114	3:35 pm	75.9	23.1	94.7
115	3:39 pm	90.8	12.3	94.3
116	3:42 pm	89.6	16.5	93.9
117	3:47 pm	86.1	Hover	93.4
118	3:52 pm	66.8	Hover	93.0
119	3:56 pm	51.5	Hover	92.5
120	4:05 pm	36.3	8.7	62.3
121	4:09 pm	35.1	17.5	61.8
122	4:13 pm	31.1	21.1	61.4
123	4:16 pm	30.8	32.4	60.9
124	4:21 pm	25.6	40.1	60.5
125	4:25 pm	40.5	12.3	60.0
126	4:29 pm	40.8	16.5	59.6
127	4:33 pm	41.5	23.7	59.2
128	4:37 pm	39.6	35.5	58.7
129	4:41 pm	52.1	12.3	58.3
130	4:44 pm	60.0	16.5	57.8
131	4:49 pm	49.4	23.7	57.4
132	4:52 pm	43.0	32.4	56.9
133	4:56 pm	46.0	Hover	56.5
134	5:00 pm	31.7	Hover	56.0
135	5:06 pm	23.2	Hover	55.6

Table 7. Test Matrix for the Blackhawk on 30 September 1994.

Run Number	Time	Height (m)	Flight Speed (m/sec)	Weight (kN)
136	9:58 am	33.2	5.7	80.1
137	10:01 am	32.3	7.7	79.8
138	10:04 am	34.7	26.7	79.6
139	10:08 am	33.2	32.4	79.3
140	10:11 am	33.2	39.1	79.1
141	10:15 am	51.8	14.9	78.8
142	10:19 am	53.3	20.6	78.6
143	10:23 am	53.3	26.7	78.3
144	10:27 am	52.1	32.4	78.1
145	10:32 am	52.4	41.7	77.8
146	10:37 am	63.7	10.3	77.6
147	10:41 am	67.7	16.5	77.3
148	10:45 am	68.6	24.7	77.1
149	10:49 am	68.6	34.0	76.8
150	10:52 am	69.8	44.8	76.6
151	10:57 am	32.9	Hover	76.4
152	11:08 am	35.1	24.2	55.6
153	11:12 am	37.5	7.2	55.4
154	11:17 am	36.6	Hover	55.1

Table 8. Test Matrix for the Skycrane on 1 October 1994.

Run Number	Time	Height (m)	Flight Speed (m/sec)	Weight (kN)
155	11:51 am	94.5	4.1	160.1
156	11:56 am	100.6	9.3	159.2
157	12:00 pm	109.7	21.1	158.3
158	12:03 pm	105.8	33.4	157.5
159	12:09 pm	115.5	5.7	156.6
160	12:15 pm	116.4	8.7	155.7
161	12:18 pm	123.4	22.1	154.8
162	12:24 pm	102.4	Hover	153.9
163	12:29 pm	87.8	Hover	153.0
164	1:28 pm	41.5	4.6	115.6
165	1:32 pm	43.6	11.3	114.8
166	1:35 pm	44.2	20.6	113.9
167	1:38 pm	35.1	34.0	113.0
168	1:41 pm	32.0	41.7	112.1
169	1:46 pm	39.6	4.6	111.2
170	1:49 pm	34.7	9.8	110.3
171	1:52 pm	36.3	20.6	109.4
172	1:54 pm	25.3	29.3	108.5
173	1:58 pm	27.1	40.6	107.6
174	2:09 pm	56.4	4.6	106.8
175	2:12 pm	60.0	9.8	105.9
176	2:16 pm	63.1	23.7	105.0
177	2:19 pm	49.4	34.5	104.1
178	2:22 pm	41.5	41.2	103.2
179	2:26 pm	57.3	Hover	102.3
180	2:30 pm	40.8	Hover	101.4
181	2:35 pm	31.7	Hover	100.5

3. DATA REDUCTION AND INTERPRETATION

The purpose of the field study was to collect data that captured the helicopter downwash and its subsequent induced surface sidewash effects, outward from the aircraft flight path. The 181 trials summarized in Tables 1 to 8 clearly contain a great deal of information available for processing. The step-by-step way in which these data were reduced and interpreted is now detailed.

The analog-to-digital hardware sampled 100 data points per second, cycling through the 32 anemometer readings (the readings were therefore recorded 0.34 sec apart). A large amount of noise appeared to be present in the raw signals; while this is not uncommon with field data, it required us to do some conditioning of the data to recover the trends more clearly. To illustrate, we display two sets of velocity traces, from a hover simulation (Figures 2a, 2b and 2c) and from a slow forward flight over the tower grid (Figures 3a, 3b and 3c).

Several common observations may be made from an inspection of these figures. Figures 2a and 2b, and 3a and 3b, display the left and right velocity time histories, identified here for convenience as the sides of the tower grid where the raw data gave negative and positive horizontal velocities, respectively. Note that what happened in Figures 3a and 3b for only a short time period (the large spike in velocity, followed by a decay back to the original velocity level before the passage of the helicopter, here near 75 to 80 seconds) maintained itself for a much longer period of time in Figures 2a and 2b because of the presence of the hovering helicopter. Since these signals display the total horizontal velocity, they also contained the ambient atmospheric wind speed. To isolate only on the helicopter effects, this mean wind must be subtracted from the signal (in these two cases, the mean wind values are 0.4 m/sec and -1.3 m/sec respectively).

The other interesting observation is that the left and right signals did not give the same velocity levels. In the idealized world of modeling, it would be assumed that the induced horizontal sidewash velocity generated by a helicopter was identical left and right. That was not the case here, although Figures 2a and 2b show a close correlation with maximum value. Also, these figures show that the helicopter hovered approximately 70 seconds before moving off.

Figures 2c and 3c display the downwash under the helicopter. In the normal flyover case (Figure 3c) the downwash was seen almost as a spike in the data as the helicopter passed overhead. The hover case (Figure 2c) displayed the downwash more easily (later calculations will show that the analytical downwash velocity from these two helicopters should be 17.9 m/sec for Figure 2c and 8.6 m/sec for Figure 3c). Because the grid was rather sparse, and the helicopter rotor radii smaller than the spacing between towers, it was considered fortuitous (lucky) when a vertical anemometer captured the expected downwash velocity level. Because the ambient atmosphere so close to the level ground should not contain any vertical velocity component, we did not remove any background value from the traces shown in Figures 2c and 3c.

These (typical) raw velocity signals must then be conditioned as a prelude to examination. Since each reading was a slight time difference from its partner readings, we felt it necessary to put them on more of an equal footing. To do so, we first averaged every three readings from each anemometer to produce 1 second average data. This approach tended to smooth the data somewhat, and make the data reduction process a bit easier.

Next, we needed to subtract the mean ambient horizontal wind speed from the anemometer data. To do so, we averaged together each of the six anemometer readings at each height for 30 seconds at the beginning of each trial (at least 30 seconds, and more like 40 or 50 seconds, of data were recorded before the helicopter approached the tower grid -- just for this purpose). Each of the four tower levels then produced an average ambient horizontal wind speed, which could be subtracted from each anemometer time history. After subtraction, what results should be the trace of the effects of the helicopter alone. The average horizontal wind speed at each of four heights could also be used to extract the turbulence level in the atmosphere (assuming a logarithmic profile shape to the ambient wind speed), should we have occasion to examine the turbulence at a later date. It may be seen from Tables 1 to 8 that the trials were conducted throughout the day without regard to atmospheric stability. Temperature readings were made by the USDA Forest Service, but these data are not presently available.

We then recovered the minimum and maximum induced sidewash velocities (where the convention here is negative for left side and positive for right side). Generally, these velocities were found on the lower height anemometers.

If the actual helicopter wakes behaved as they are typically modeled (Figure 4), then we would expect a column of air swept downward by the rotation of the rotor blades toward the ground. As this high-speed air nears the surface, it must abide by the solid boundary it is approaching and separate left and right away from the helicopter centerline. Classical helicopter theory suggests that a dividing streamline exists, separating the ambient air (below it) affected by the wake of the helicopter, from the quiescent air (above it) unaffected by the presence of the helicopter. Within this model, the maximum induced sidewash velocity generated by the helicopter would approximate the helicopter downwash speed, until atmospheric effects (mostly formation of the boundary layer beneath the spreading sidewash velocity, and turbulence) act on the flow field to diffuse and dissipate it. In the case of helicopters in forward flight, a gust front of sorts should exist at the front of the spreading sidewash velocity, illustrated most easily by the movement of the maximum induced sidewash velocity outward from the helicopter centerline and across the tower grid.

With the locations of the minimum and maximum induced sidewash velocities known, we could then deduce the decay of these induced velocities back to their near-zero levels. Figure 3a most clearly shows the anticipated behavior: the (in this case) minimum value of the induced sidewash velocity gradually decays after the passage of the helicopter. This decay time period may be determined by matching an exponential decay function of the form

$$V = V_m \exp (- t / \tau) \qquad (1)$$

to the induced sidewash velocity trace (V as a function of time t), anchoring its initial value to the minimum (or maximum) value there (V_m), then by least squares determining the e-folding time constant τ (in seconds). This time constant should be representative of the sustainability of the induced sidewash velocity generated by the helicopter.

The depth of the gust front produced by the helicopter may be found by tracing the vertical profile of the induced sidewash velocity at the four anemometer positions on the outermost towers. If we were fortunate, the towers would be sufficiently high so that the last anemometer (at 13.7 m) would be above the dividing streamline. With the minimum (or maximum) induced sidewash velocity generally occurring in the lowest or

next to the lowest anemometers, we could then linearly interpolate through the vertical profile and find the height at which the induced sidewash velocity is half of its minimum (or maximum) value. We averaged over 20 seconds of data after the appearance of the largest induced sidewash velocity, merely to more clearly define the data with the most likelihood of giving good results. This layer depth (in m) should be representative of the height of the induced sidewash velocity front passing outward from the helicopter.

The fourth parameter of interest is the speed at which the minimum (or maximum) induced sidewash velocity passes through the tower grid. To recover this result, we examined the times at which the largest induced sidewash velocities were exhibited at the outermost towers, and divided this average into the distance between towers (18.3 m) to determine a representative grid speed of the moving front (in m/sec).

To present these results, we examined how the several parameters from the seven helicopters of different sizes and weights may be nondimensionalized. Quite obviously, the relevant length scale is the rotor radius R. The relevant velocity scale is the analytical downwash velocity, taken from actuator disk theory as

$$W = \frac{1}{R}\left[\frac{W_t}{2\pi\rho}\right]^{1/2} \tag{2}$$

where W_t is the weight of the aircraft and ρ is the air density. Equation 2 may be applied to the base weights of the seven aircraft (given previously) to obtain the following values for the normalizing variables:

Helicopter Type	Rotor Radius (R in m)	Downwash Speed (W in m/sec)
Bell 205H	7.4	8.85
Bell 206B	5.5	6.12
Blackhawk	8.0	10.80
Boeing Vertol BV-107	7.6	14.79
Chinook CH-47	9.1	12.88
Sikorsky S-61	9.4	11.17
Skycrane	11.0	13.14

Clearly, time may be made nondimensional by multiplying by W and dividing by R. Four sets of plots are presented for each of the seven helicopters in Figures 5 through 11: the average Induced Surface Velocity (averaging the minimum and maximum induced sidewash velocities found in the data); the average least-squares Time Constant $\tau W/R$; the average Layer Depth (to half the maximum induced sidewash velocity); and the average Frontal Grid Speed, all plotted against the normalized Helicopter Speed.

With the normalization, data from the seven helicopters appear to collapse onto roughly the same scales, with the same trends. The induced surface velocities are shown with the inclusion of the helicopter height over the tower grid (with these heights grouped in several bins). In general the trends here are correct: the induced surface velocities are

stronger for hover (near the analytical downwash velocity value), then decrease as the helicopter flight speed increases (down to a value of about 0.15W); and lower release heights give higher induced surface velocities. These data are too scattered to set any consistent curvefit through the data, so this was not done.

The other three parameters are shown with the same symbol for all helicopter heights, simply because preliminary examination showed that there were no discernible trends in these three parameters with helicopter height. The time constants all scatter around common values (the effect of the vortices formed off the rotor blades will also be a part of these time constants -- separating out the competing effects is impossible); the layer depth is consistently close to the radius of the rotor (in keeping with the analytical model); and the frontal grid speed is generally around 0.15W. A summary of the average of these three parameters for the seven helicopters gives:

Helicopter Type	Time Constant $\tau W/R$	Layer Depth / R	Frontal Grid Speed / W
Bell 205H	18.69	1.102	0.139
Bell 206B	15.93	1.329	0.239
Blackhawk	16.90	1.053	0.087
Boeing Vertol BV-107	29.77	0.996	0.127
Chinook CH-47	23.65	0.909	0.151
Sikorsky S-61	13.83	0.874	0.184
Skycrane	20.32	0.778	0.153
AVERAGE	20.34	1.005	0.142

Several of these results are consistent with the models present in AGDISP (and the near wake model in FSCBG). The anticipated induced surface velocities (approximately equal to the downwash velocity) and the layer depth (approximately equal to the rotor radius) are assumptions that are a part of these codes. The new information on decay of the maximum induced surface velocities is similar to the vortical decay model in the codes, while the movement of the gust front is information that is too complicated to fit into the codes. There is nothing here, however, that is incompatible with the existing approach to the modeling of helicopter effects on the aerial spray release of materials.

It may be seen then that this field experiment has defined the trend in expected induced surface velocities, duration of these velocities, height (or depth) of the resulting gust front, and the speed this gust front moves outward from the passing helicopter. These field results can then be inserted into the appropriate models to parameterize the effects of the passing helicopter, and infer its effect on the spread of fire, pesticides, dusts, aerosols, or other contaminants.

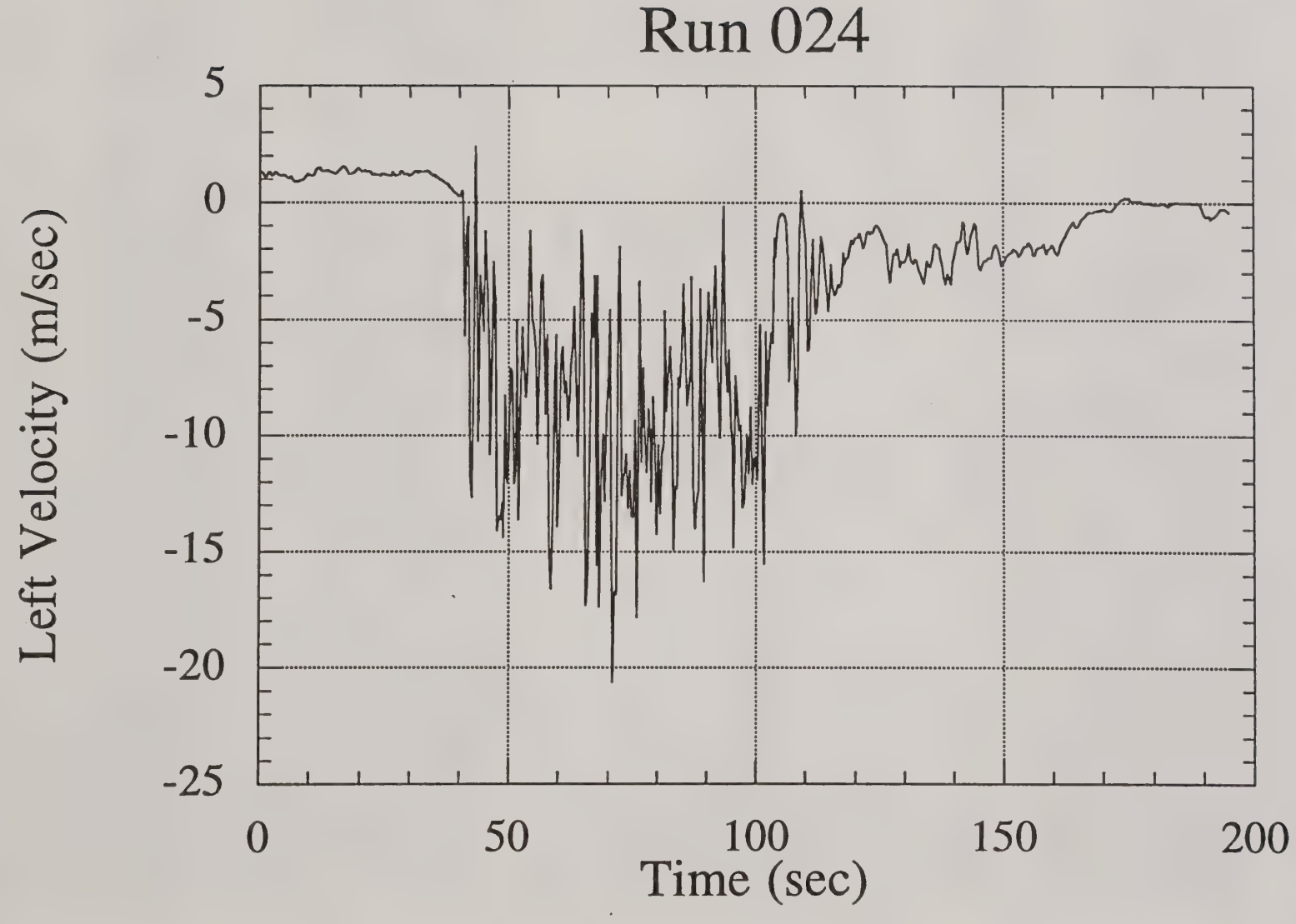

Figure 2a. Maximum velocities recorded in Run 024 -- hover raw data with no corrections -- for the left velocity time history at tower 2 anemometer level 1 (3.0 m, from Figure 1).

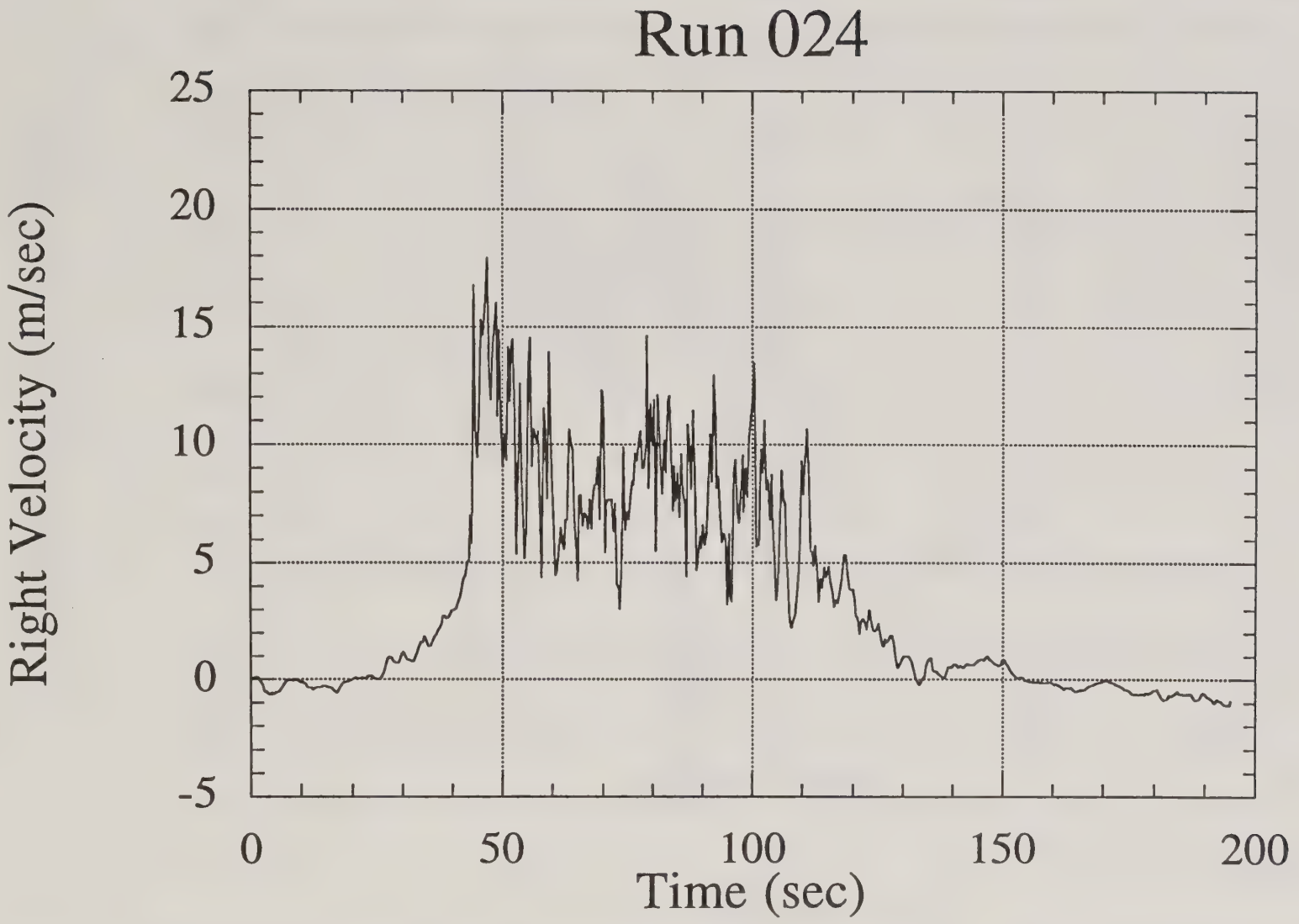

Figure 2b. Right velocity time history at tower 5 anemometer level 1.

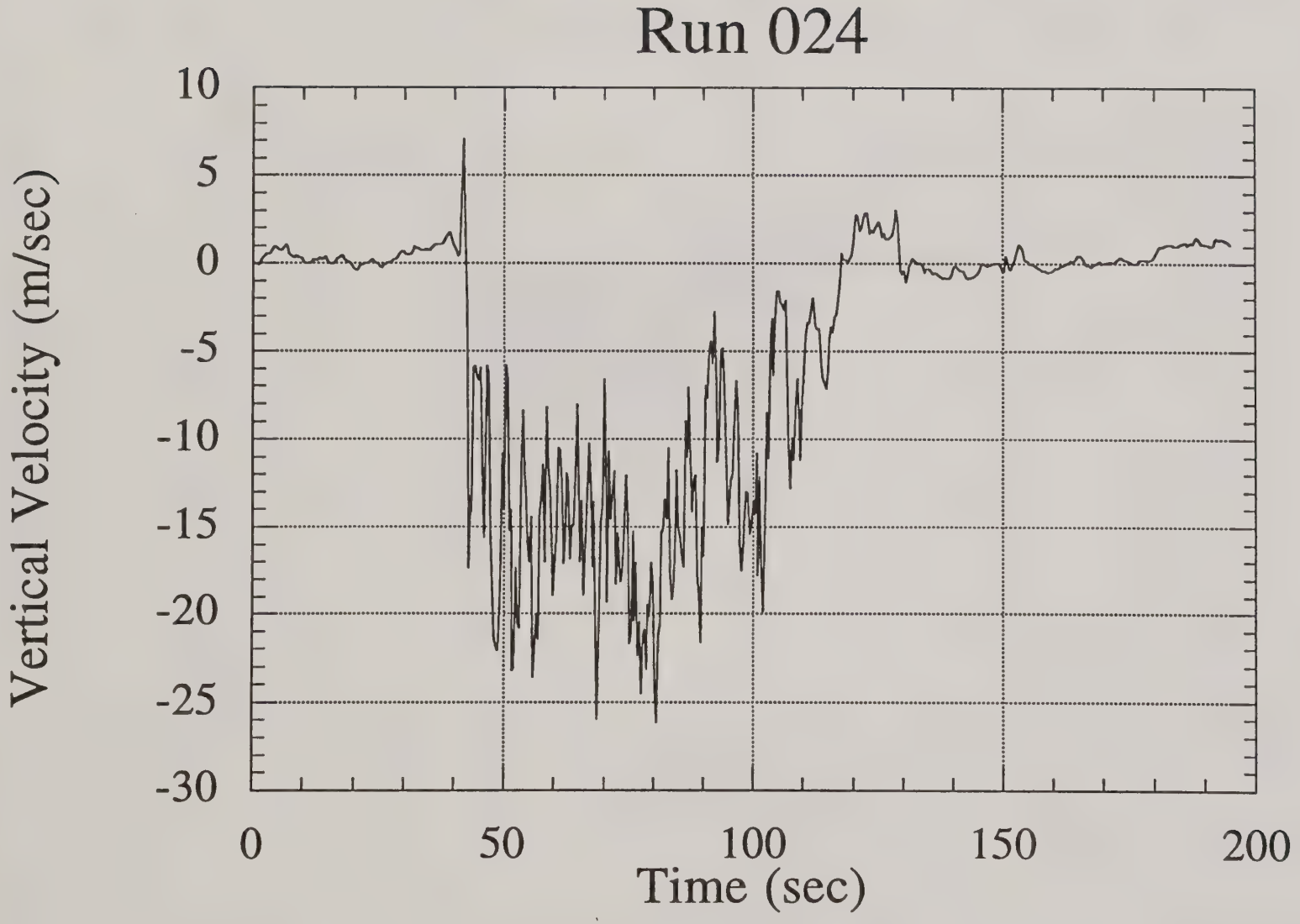

Figure 2c. Vertical velocity time history at tower 3 anemometer level 4 (13.7 m).

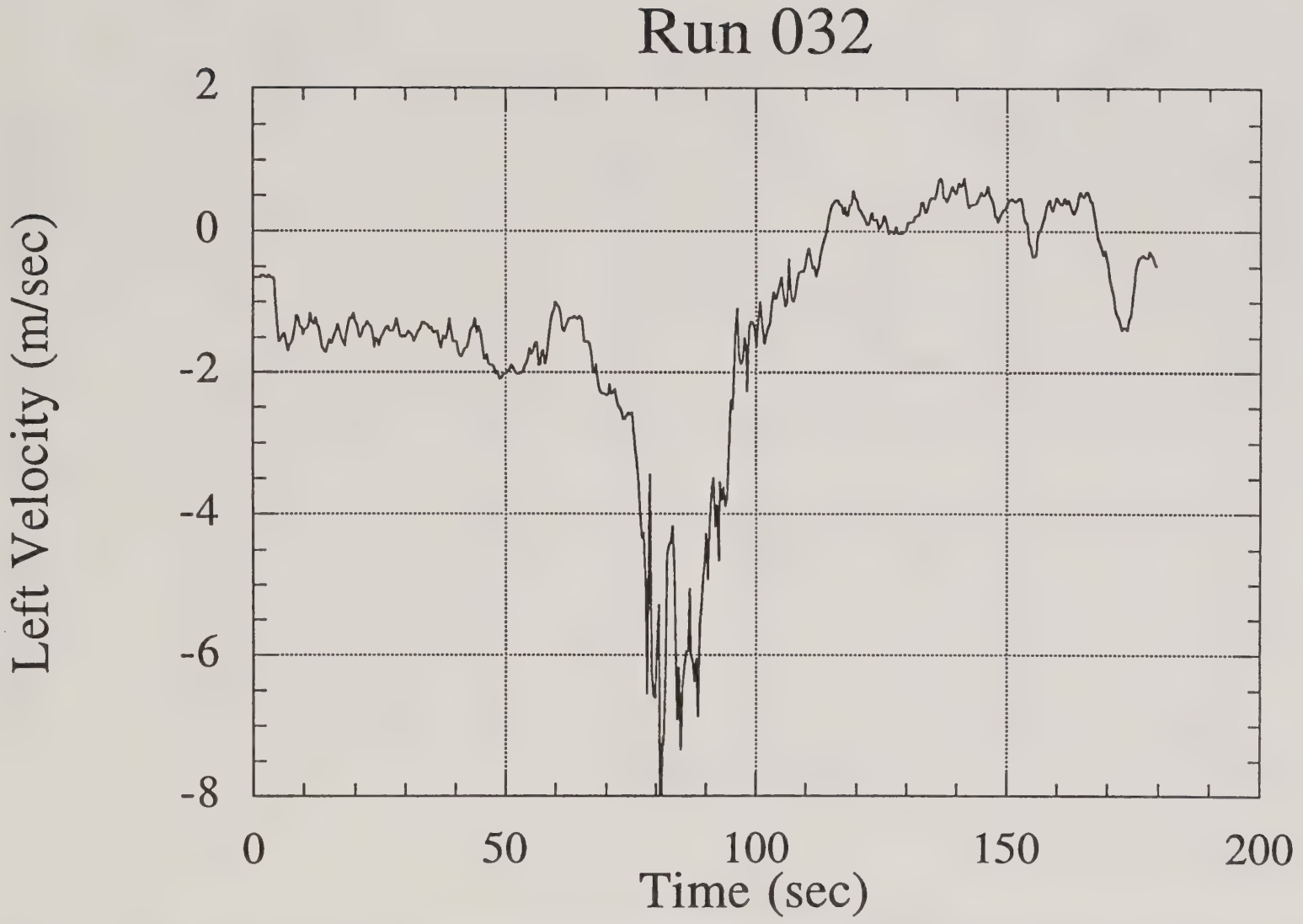

Figure 3a. Maximum velocities recorded in Run 032 -- slow forward speed raw data with no corrections -- for the left velocity time history at tower 3 anemometer lever 1.

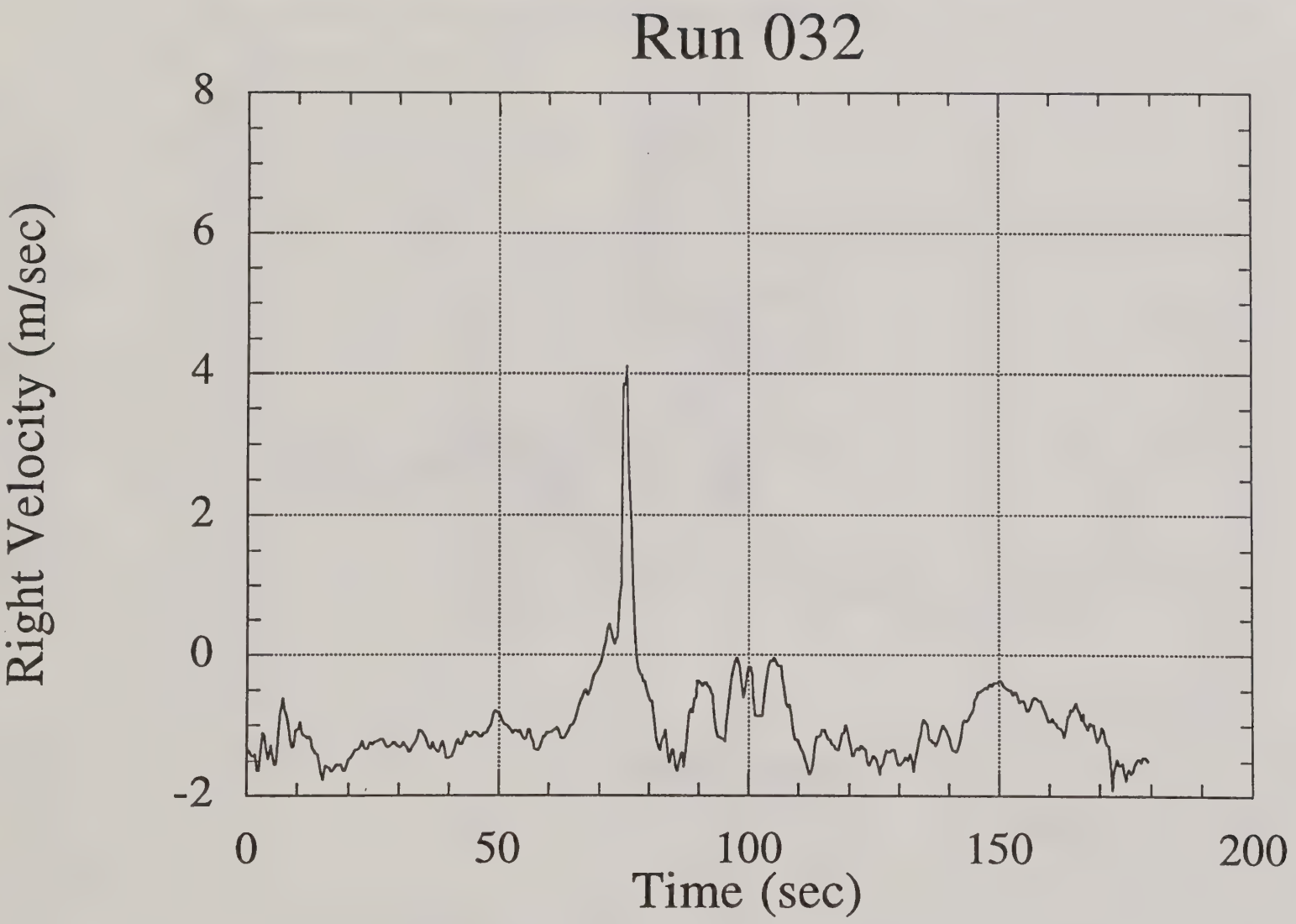

Figure 3b. The right velocity time history at tower 6 anemometer level 4.

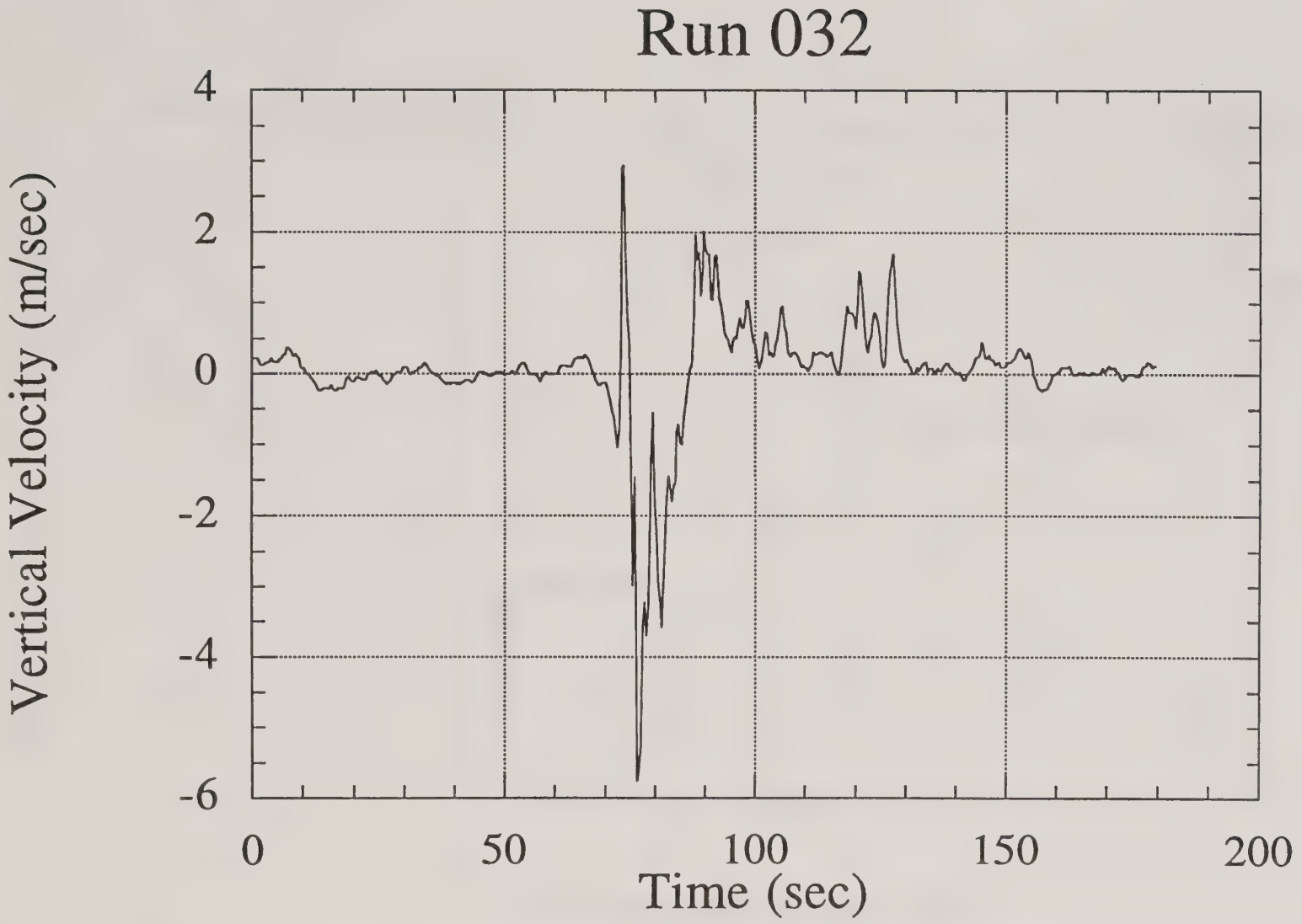

Figure 3c. The vertical velocity time history at tower 5 anemometer level 2 (6.1 m).

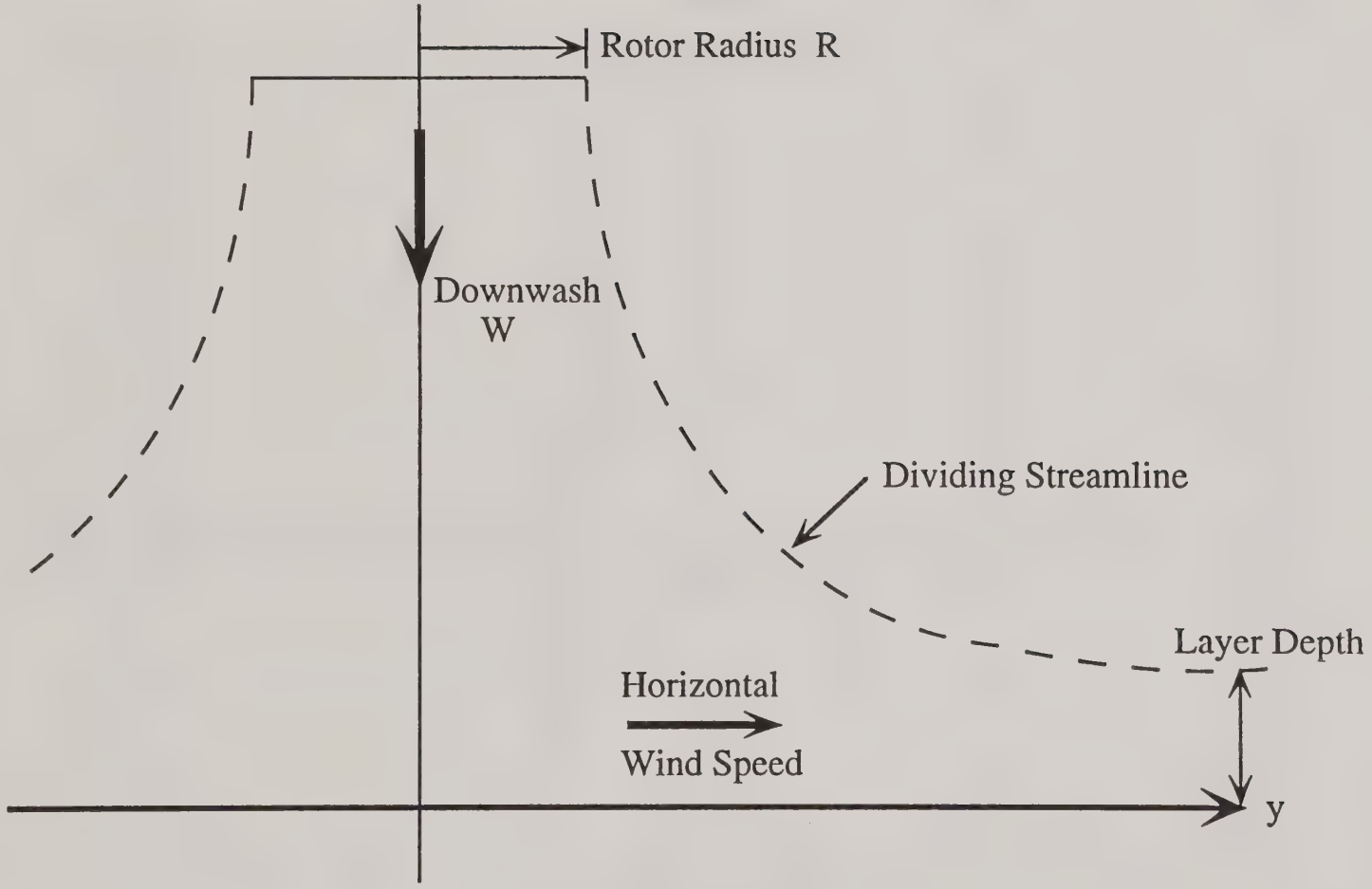

Figure 4. An idealized model representation of the effects occurring within the helicopter flow field.

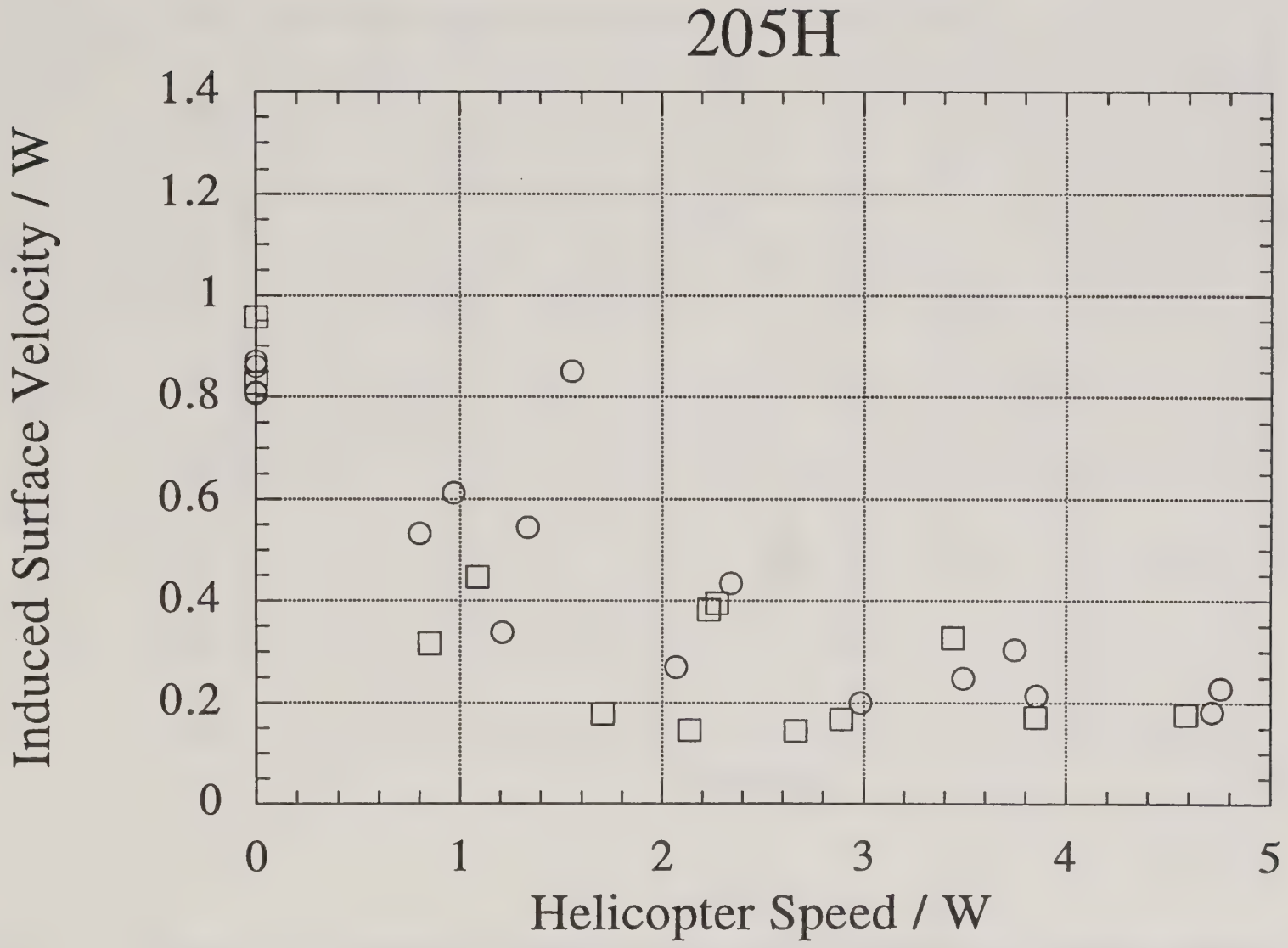

Figure 5a. Results for the Bell 205H for the average maximum induced surface velocity (normalized by the downwash speed W) plotted as a function of helicopter speed over the tower grid (also normalized by W) for 30 trial runs. Here the nominal helicopter heights are identified: less than 30 m (open circles) and greater than 30 m (open squares).

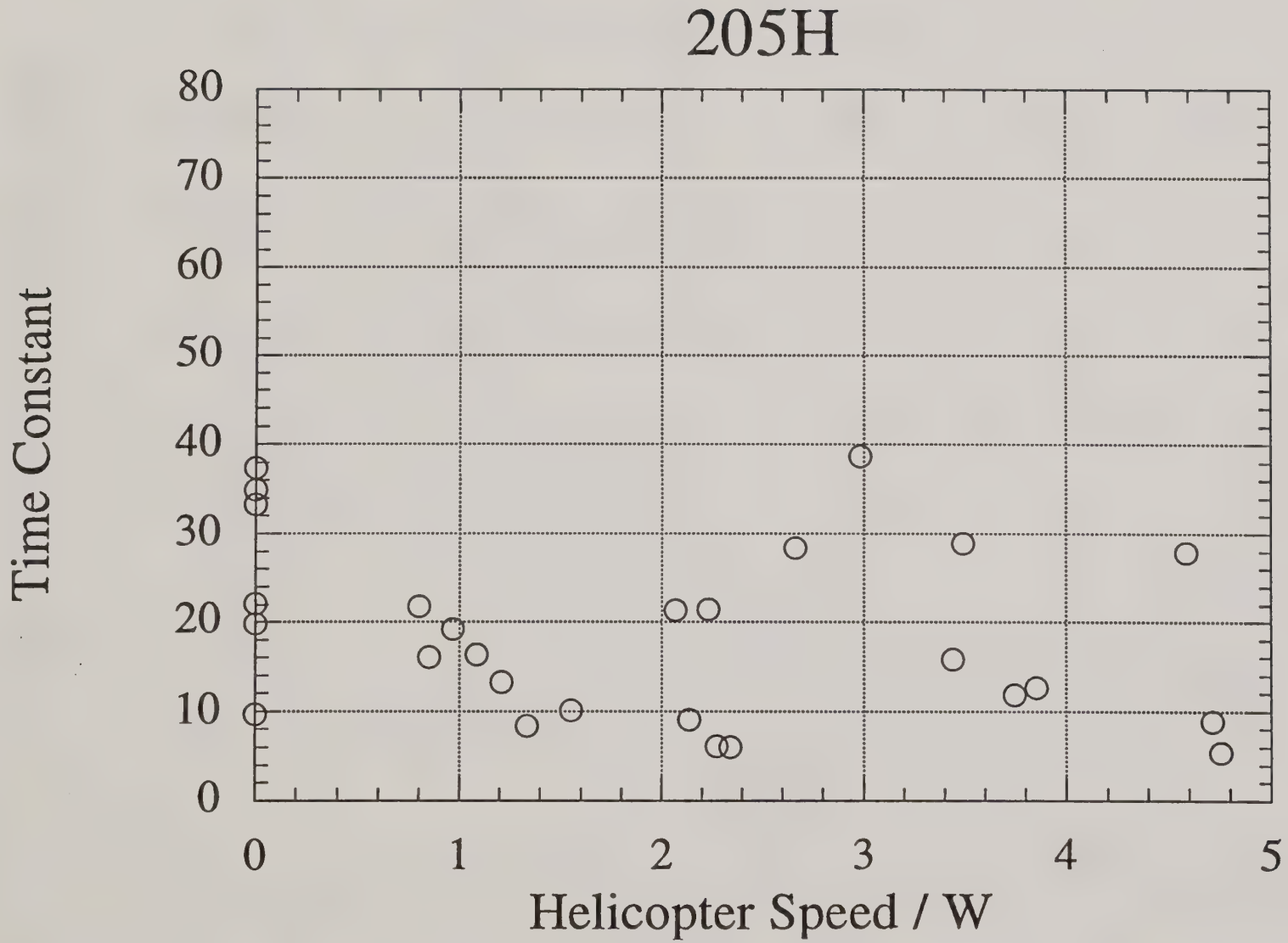

Figure 5b. The time constant τW/R for all available Bell 205H trial runs.

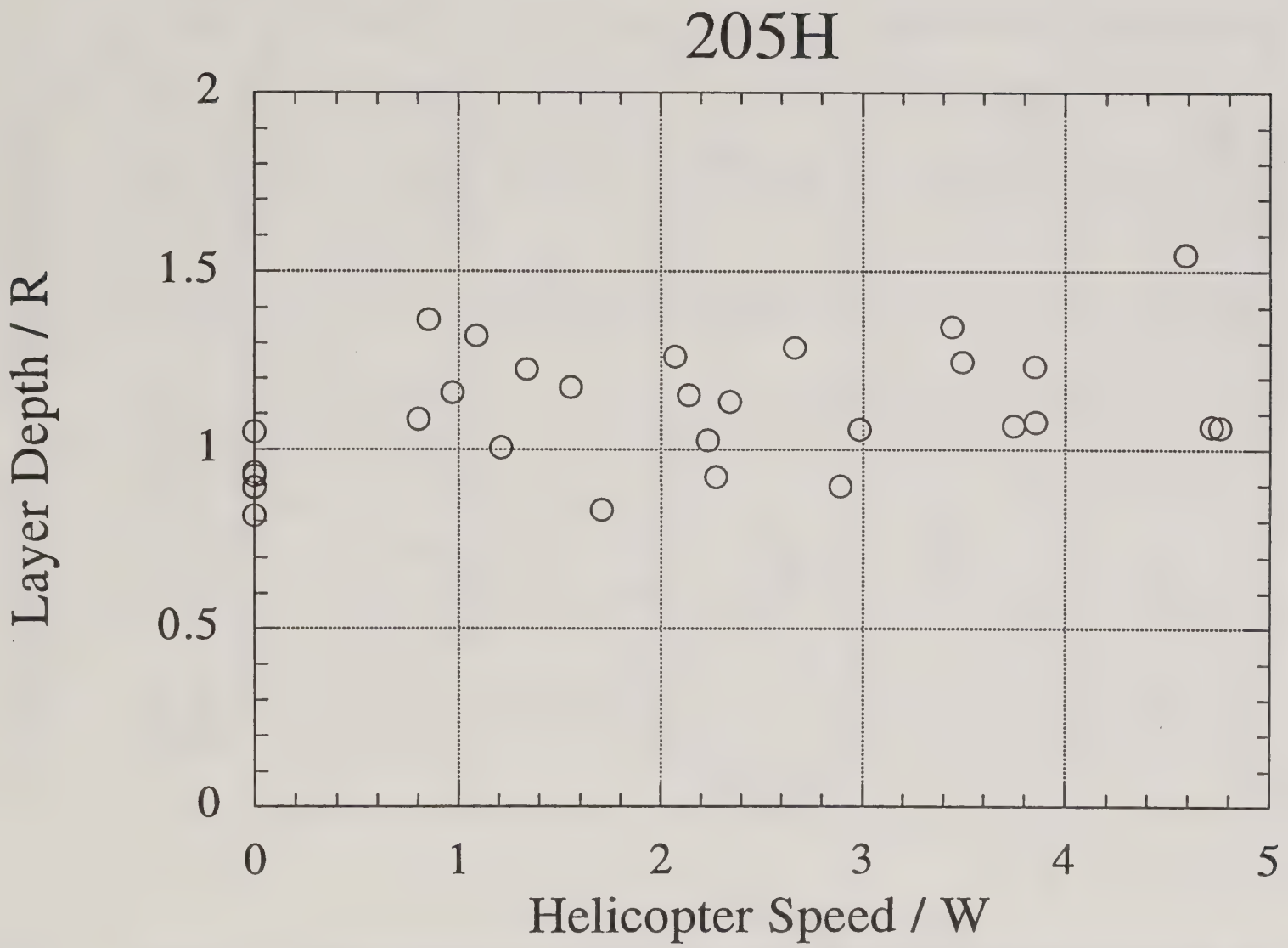

Figure 5c. The average layer depth normalized by the rotor radius R for the Bell 205H trial runs.

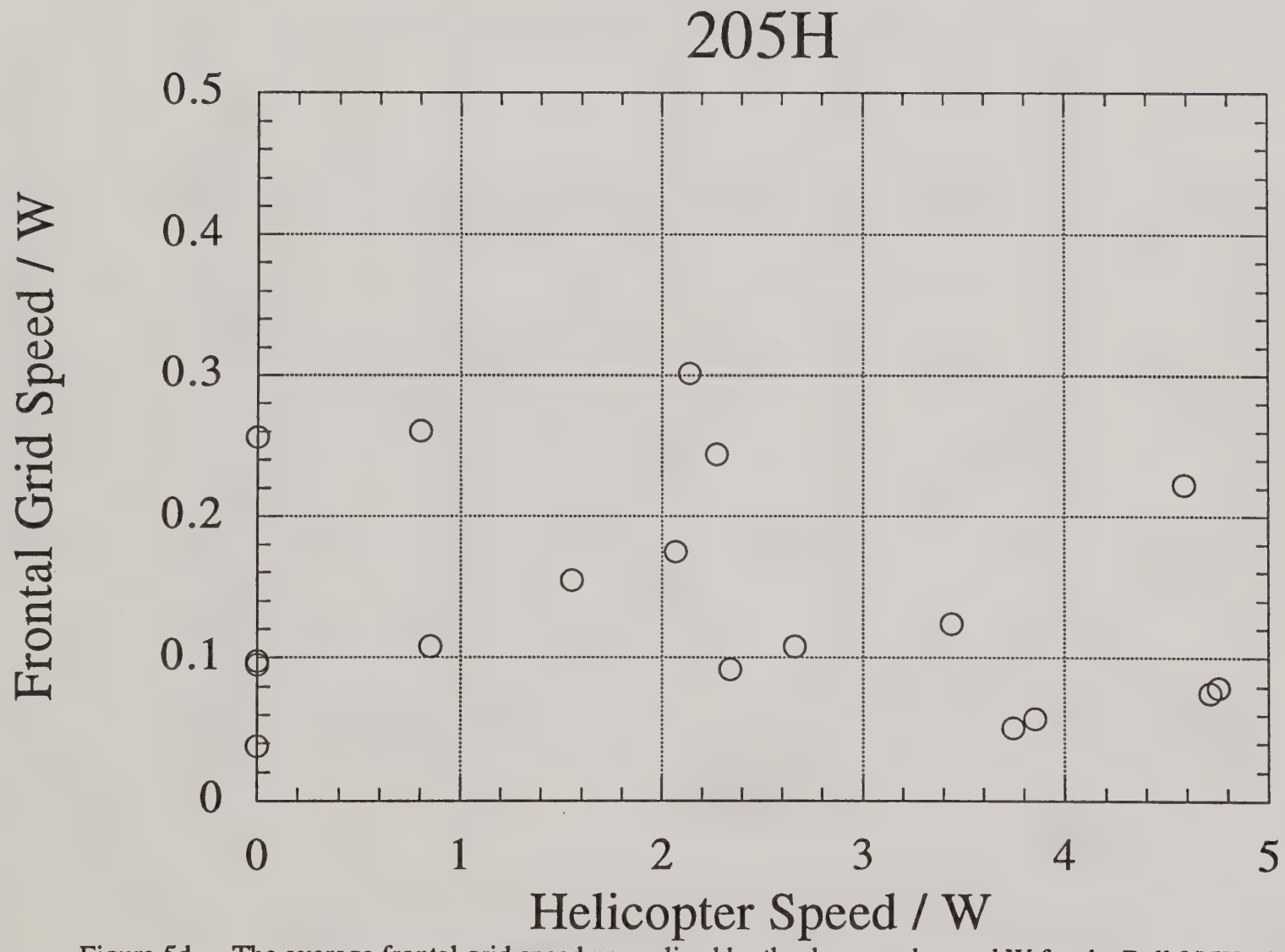

Figure 5d. The average frontal grid speed normalized by the downwash speed W for the Bell 205H trial runs.

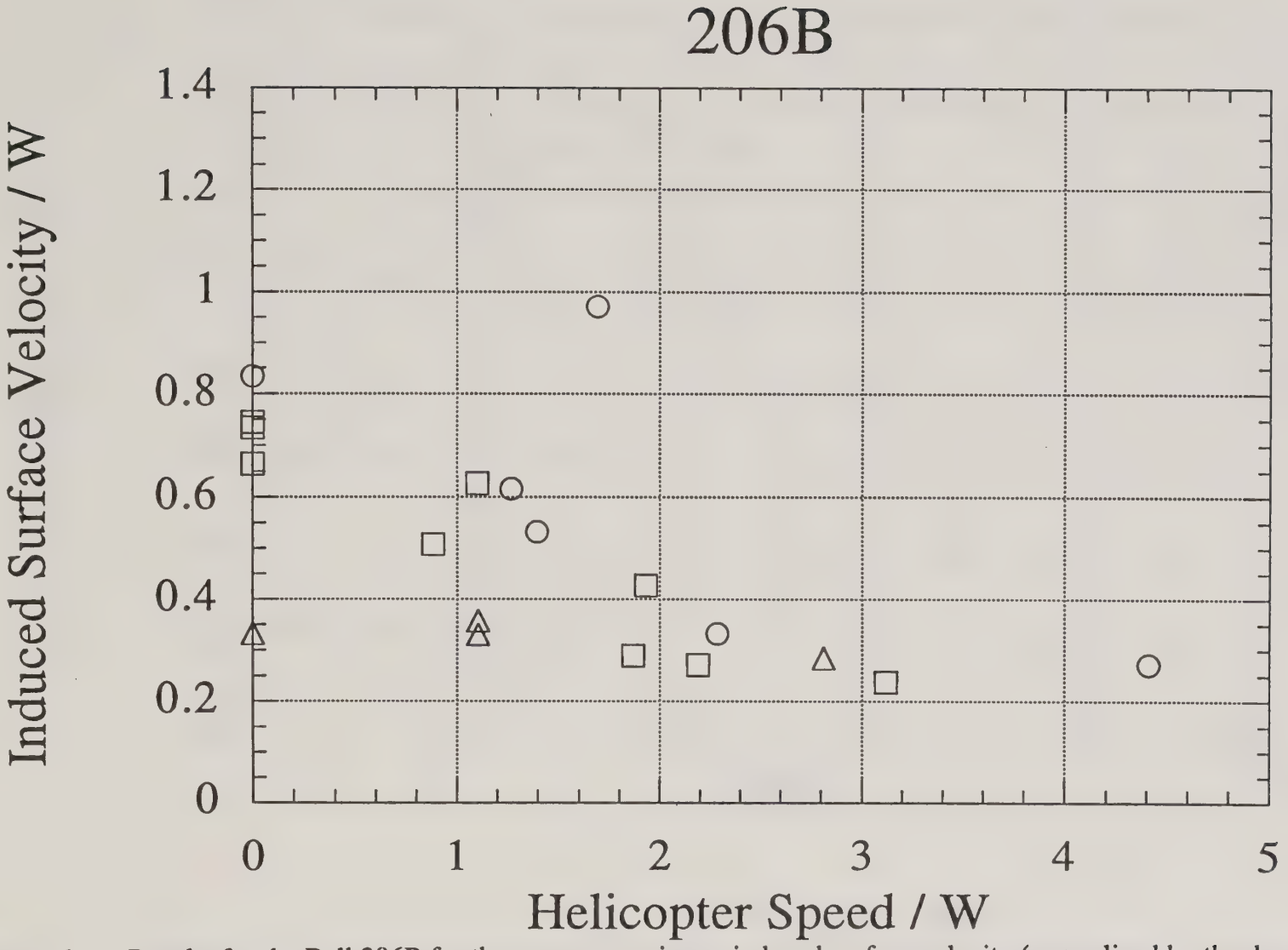

Figure 6a. Results for the Bell 206B for the average maximum induced surface velocity (normalized by the downwash speed W) plotted as a function of helicopter speed over the tower grid (also normalized by W) for 19 trial runs. Here the nominal helicopter heights are identified: less than 30 m (open circles), 30 m to 40 m (open squares) and greater than 40 m (open triangles).

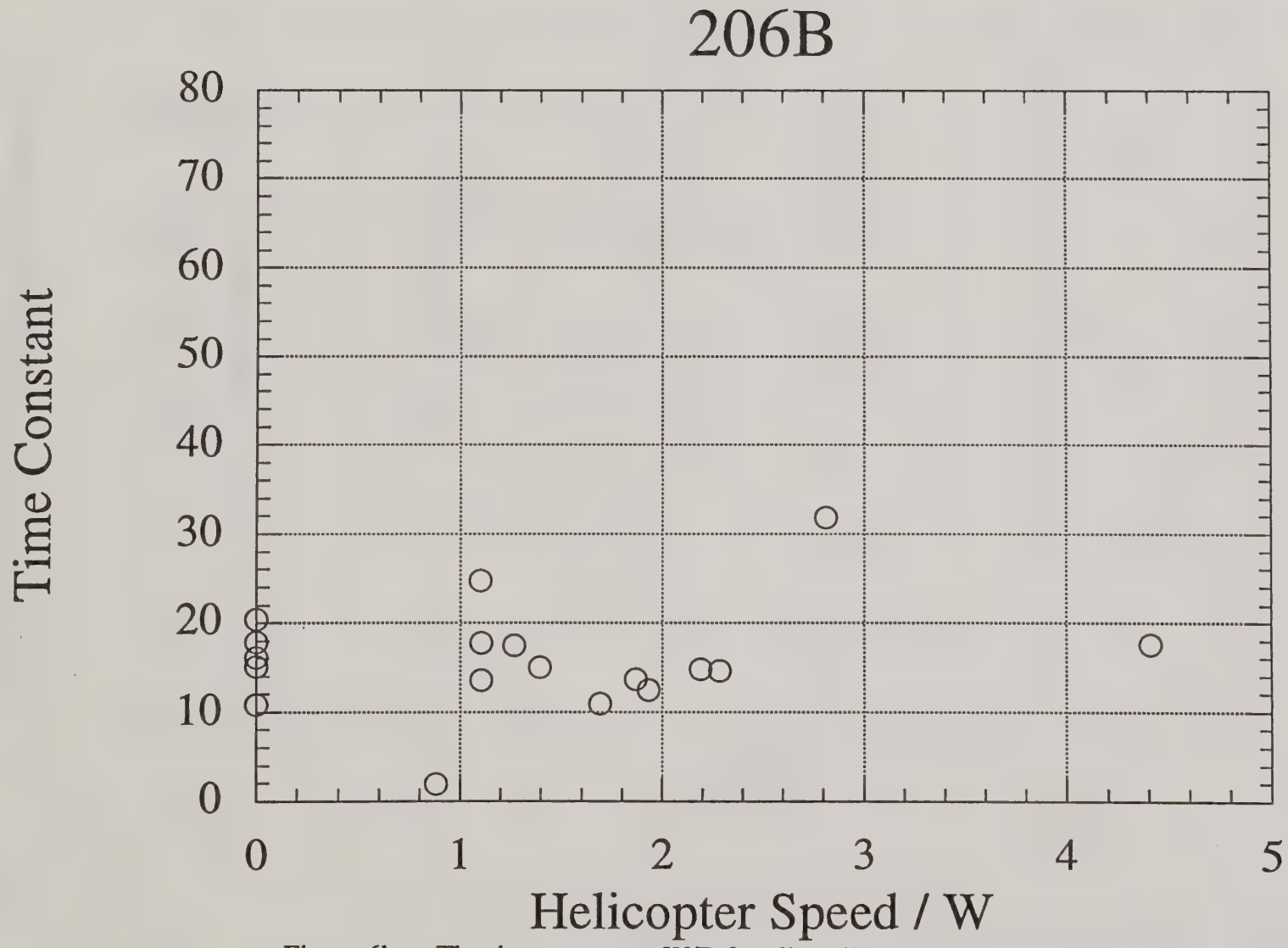

Figure 6b. The time constant τW/R for all available Bell 206B trial runs.

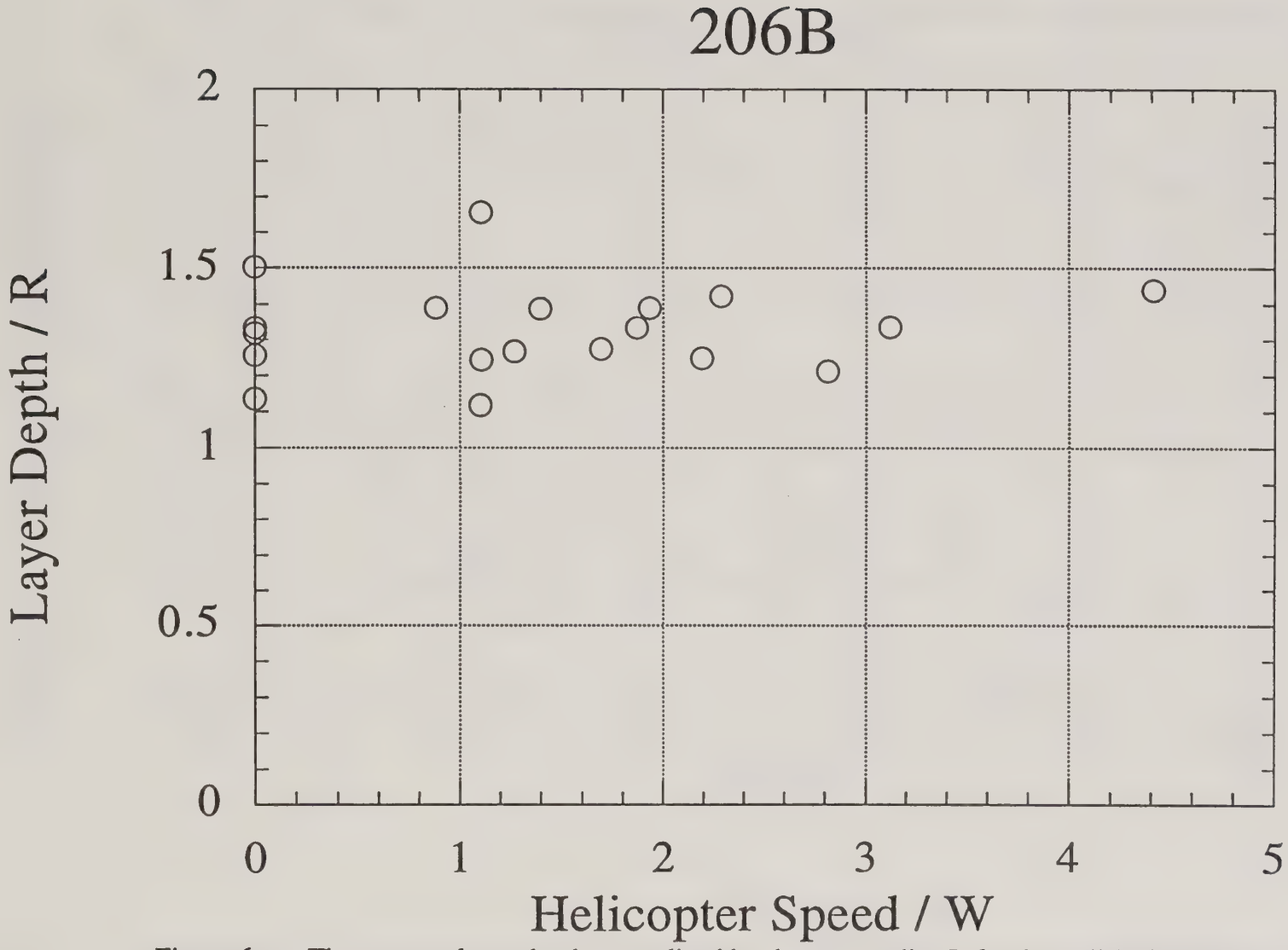

Figure 6c. The average layer depth normalized by the rotor radius R for the Bell 206B trial runs.

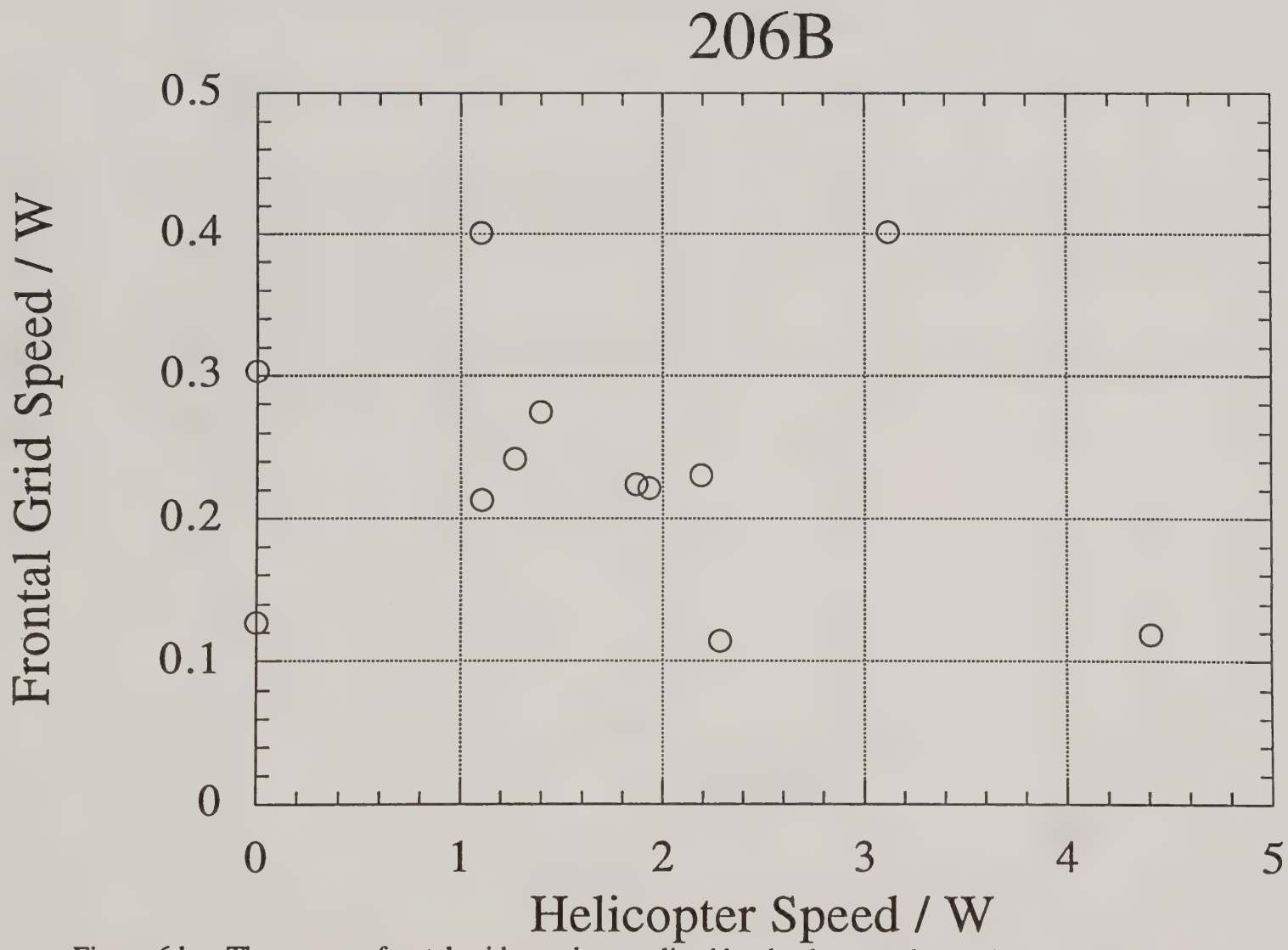

Figure 6d. The average frontal grid speed normalized by the downwash speed W for the Bell 206B trial runs.

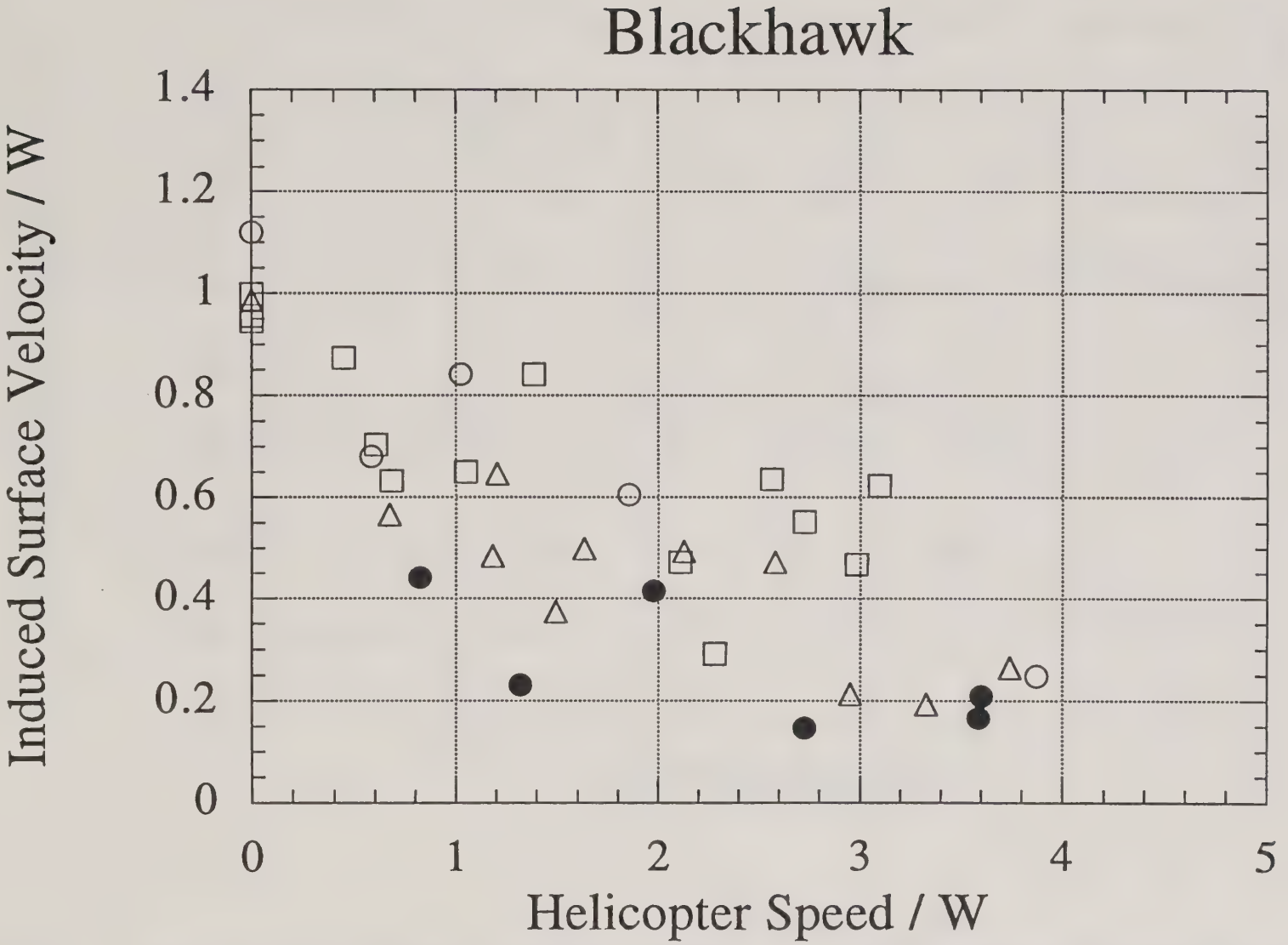

Figure 7a. Results for the Blackhawk for the average maximum induced surface velocity (normalized by the downwash speed W) plotted as a function of helicopter speed over the tower grid (also normalized by W) for 36 trial runs. Here the nominal helicopter heights are identified: less than 30 m (open circles), 30 m to 40 m (open squares), 40 m to 60 m (open triangles) and greater than 60 m (closed circles).

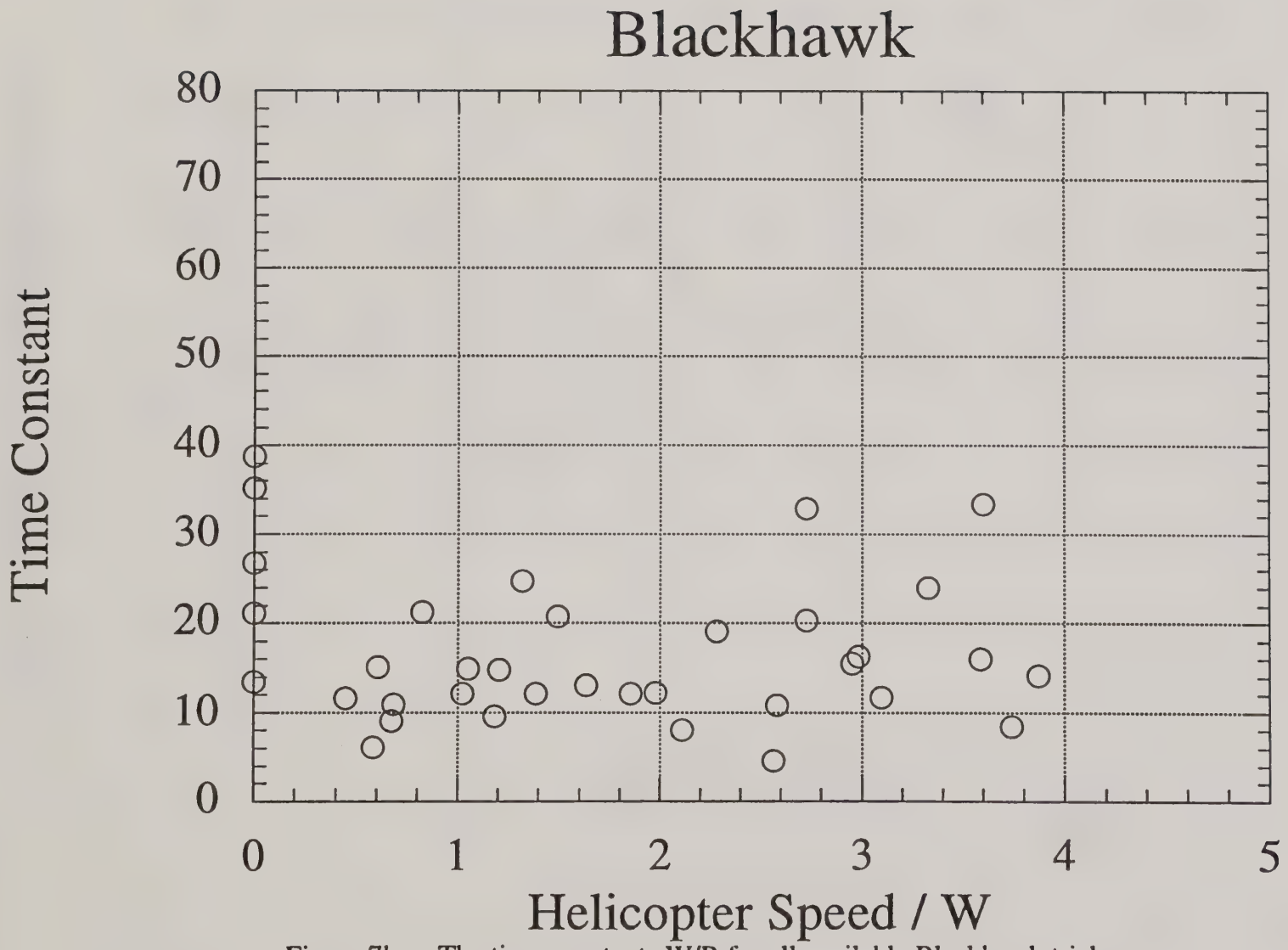

Figure 7b. The time constant τW/R for all available Blackhawk trial runs.

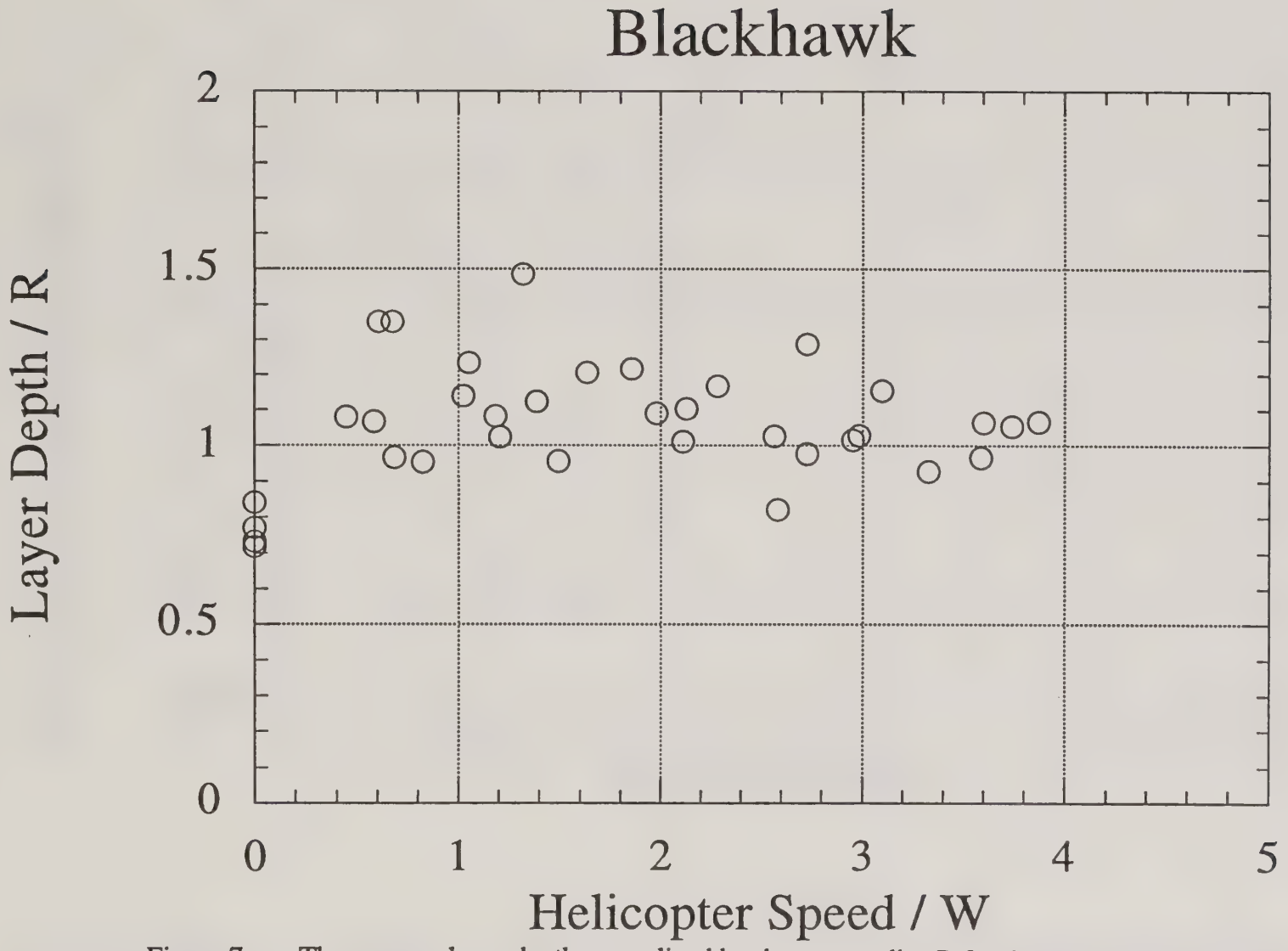

Figure 7c. The average layer depth normalized by the rotor radius R for the Blackhawk trial runs.

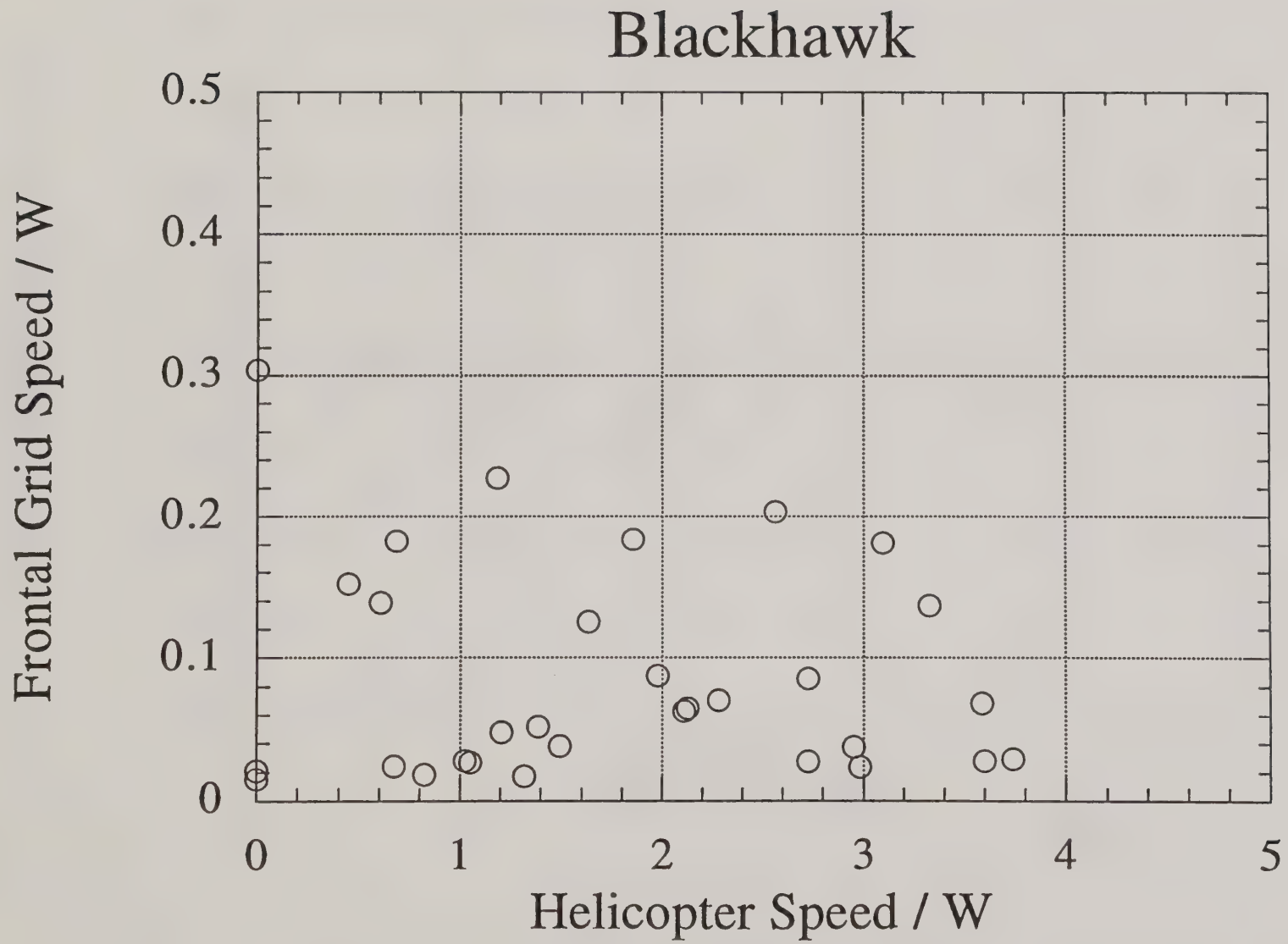

Figure 7d. The average frontal grid speed normalized by the downwash speed W for the Blackhawk trial runs.

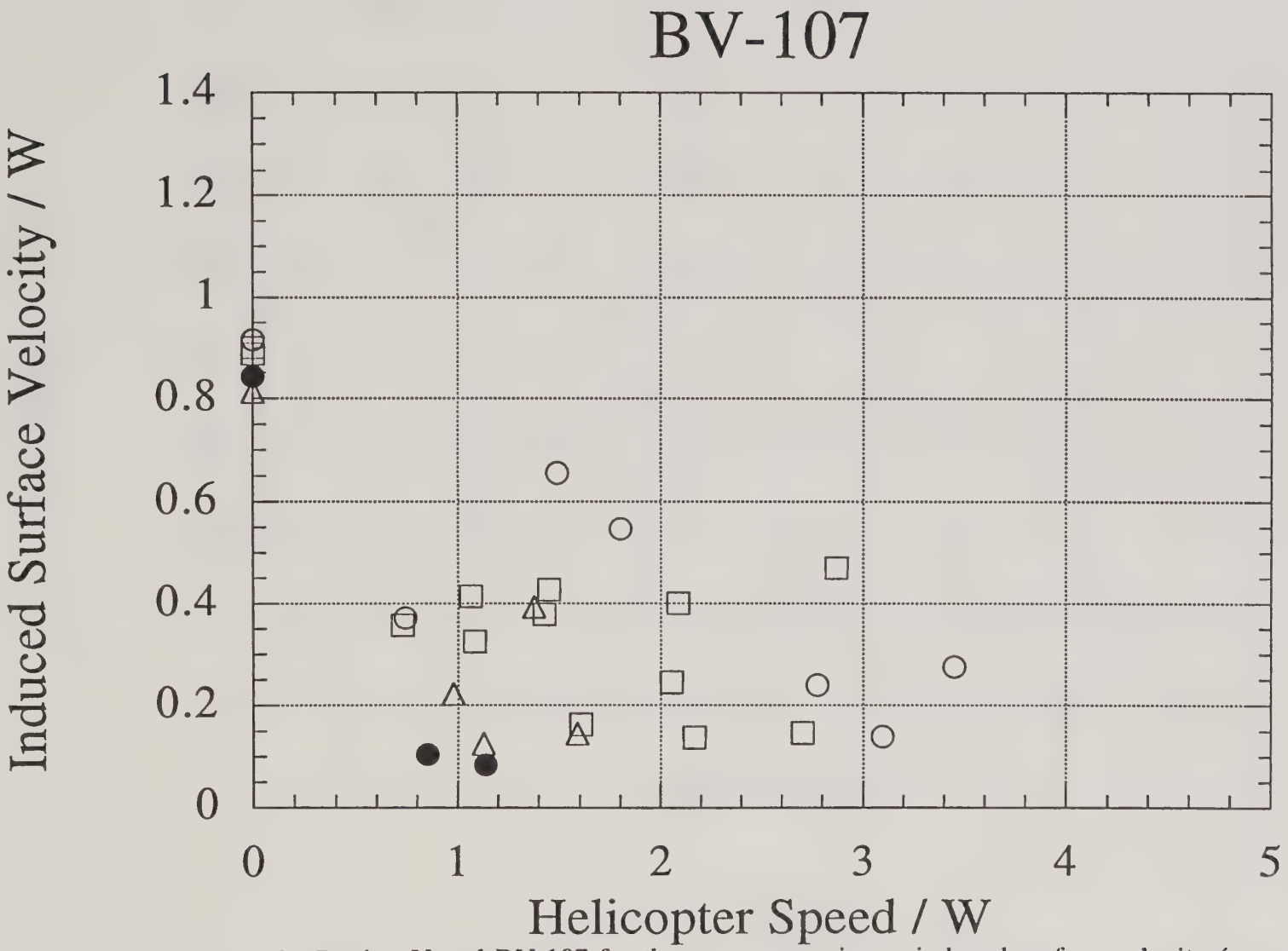

Figure 8a. Results for the Boeing Vertol BV-107 for the average maximum induced surface velocity (normalized by the downwash speed W) plotted as a function of helicopter speed over the tower grid (also normalized by W) for 29 trial runs. Here the nominal helicopter heights are identified: less than 40 m (open circles), 40 m to 60 m (open squares), 60 m to 80 m (open triangles) and greater than 80 m (closed circles).

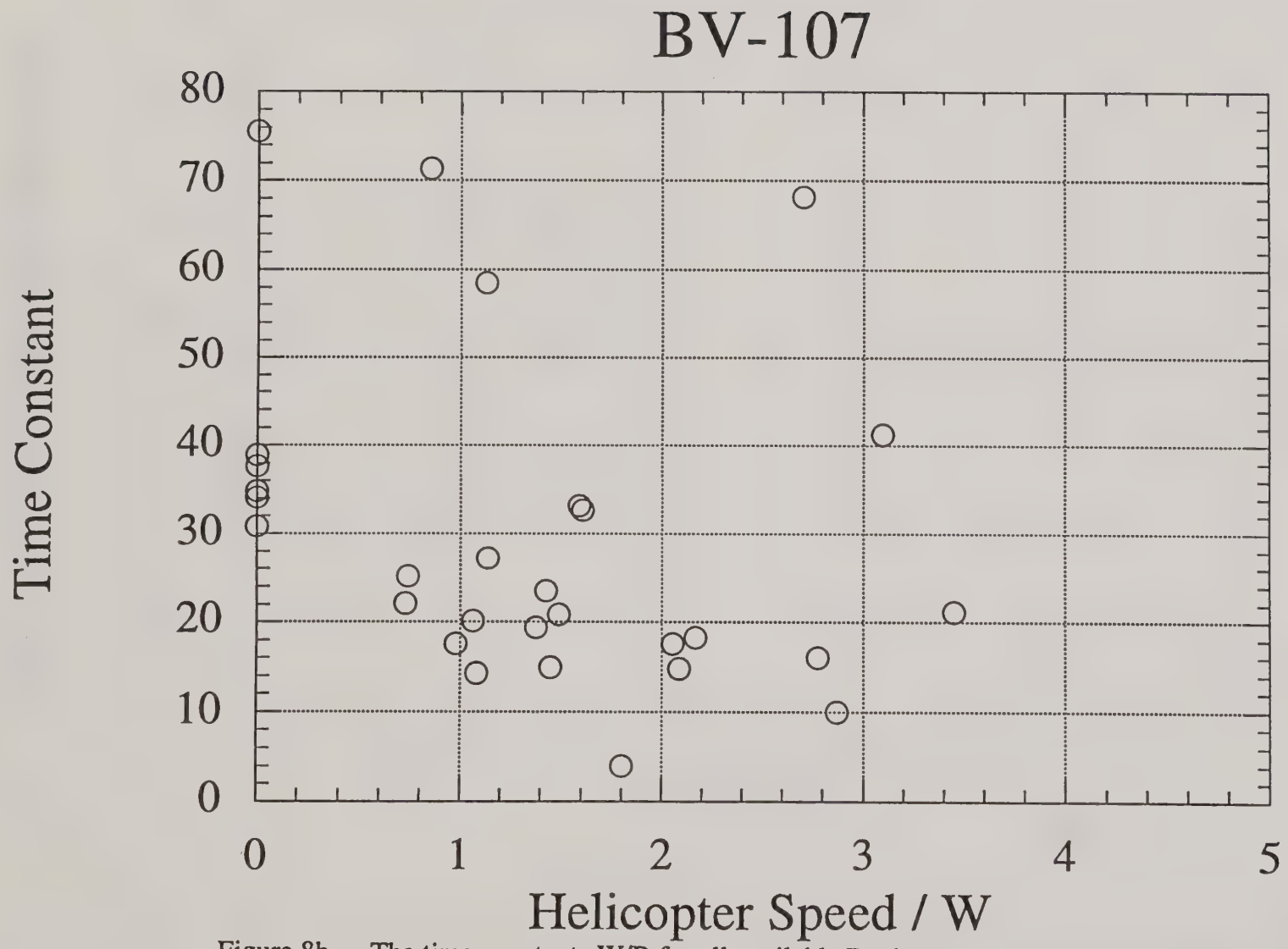

Figure 8b. The time constant τW/R for all available Boeing Vertol BV-107 trial runs.

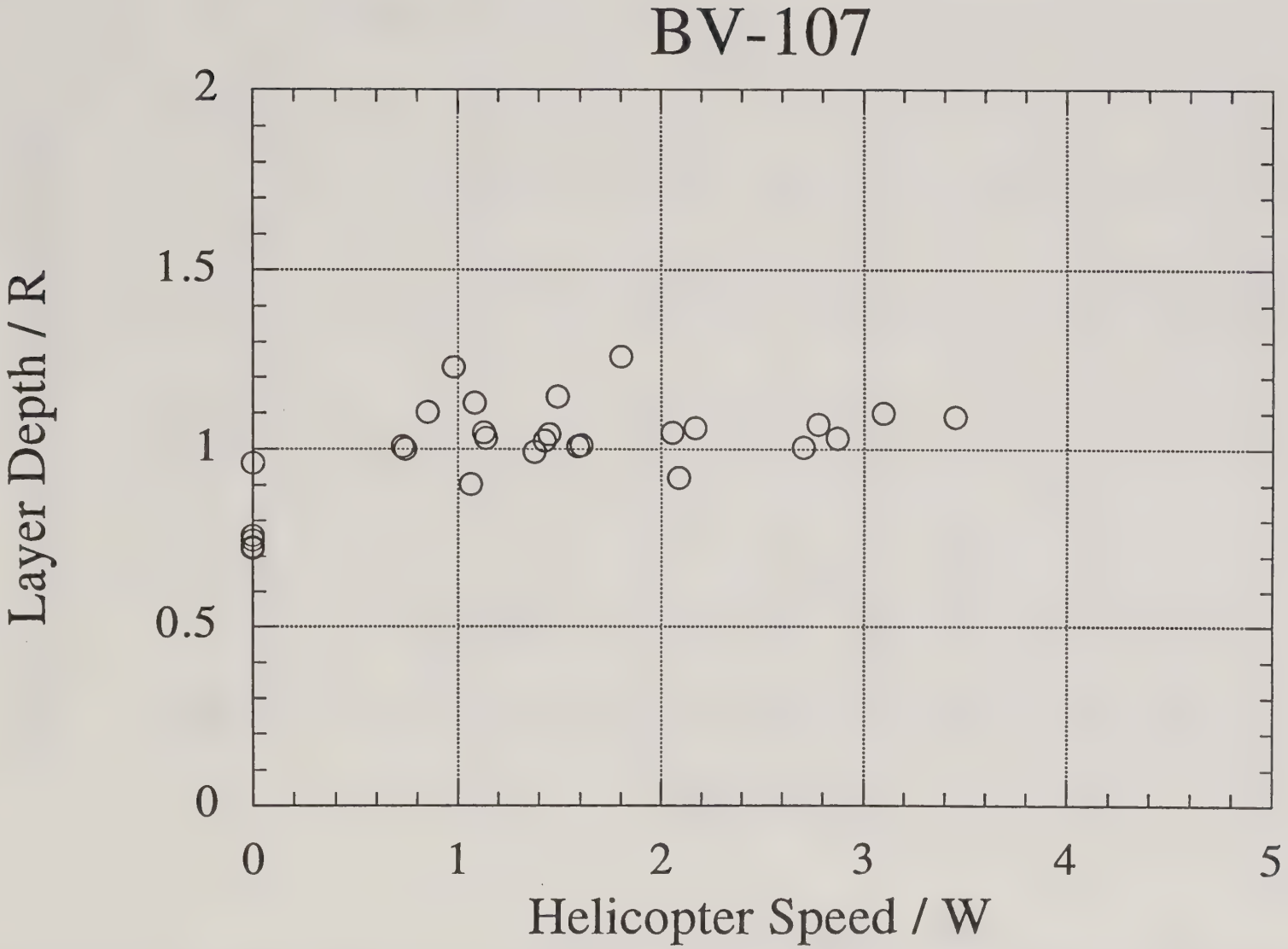

Figure 8c. The average layer depth normalized by the rotor radius R for the Boeing Vertol BV-107 trial runs.

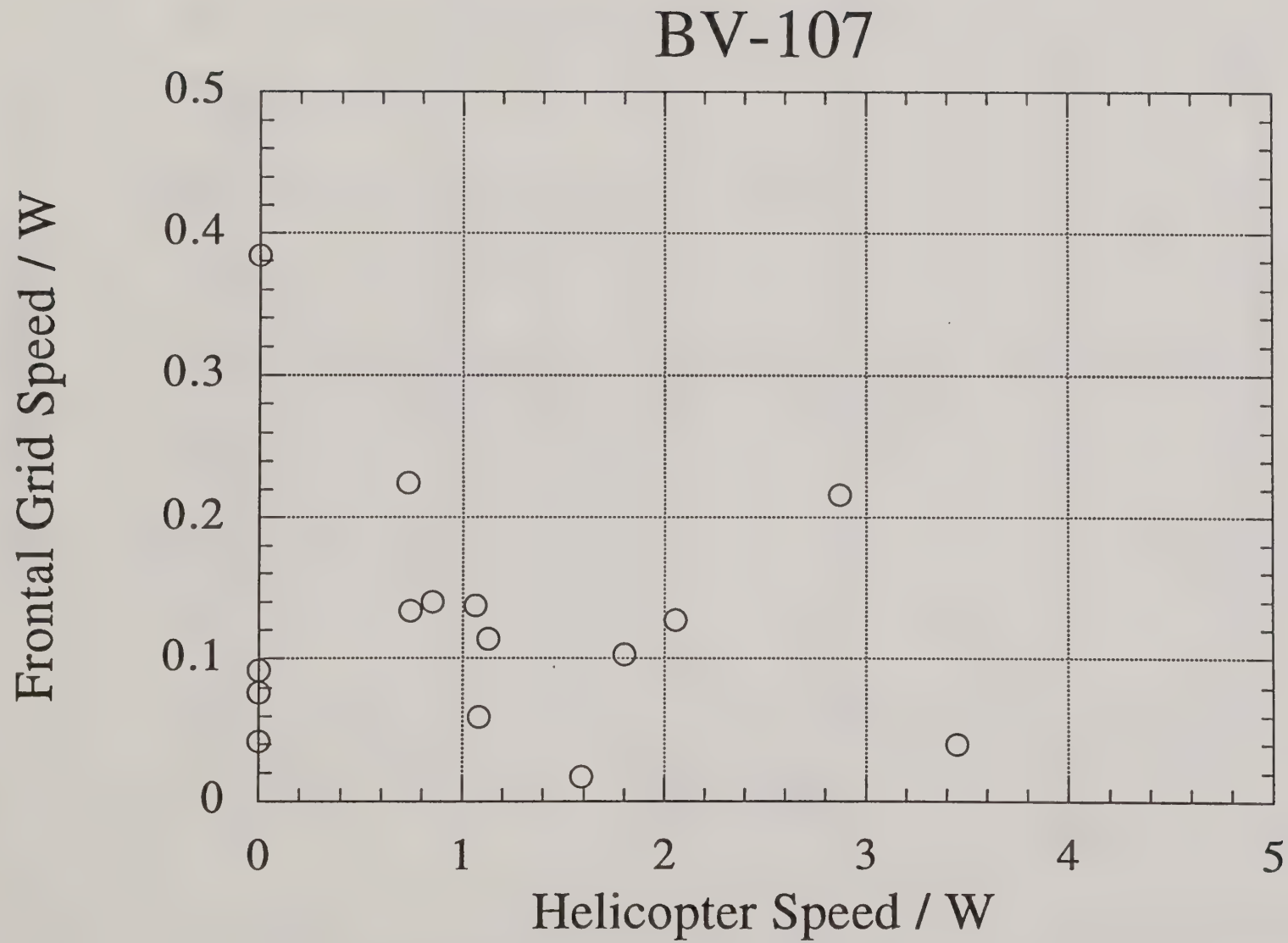

Figure 8d. The average frontal grid speed normalized by the downwash speed W for the Boeing Vertol BV-107 trial runs.

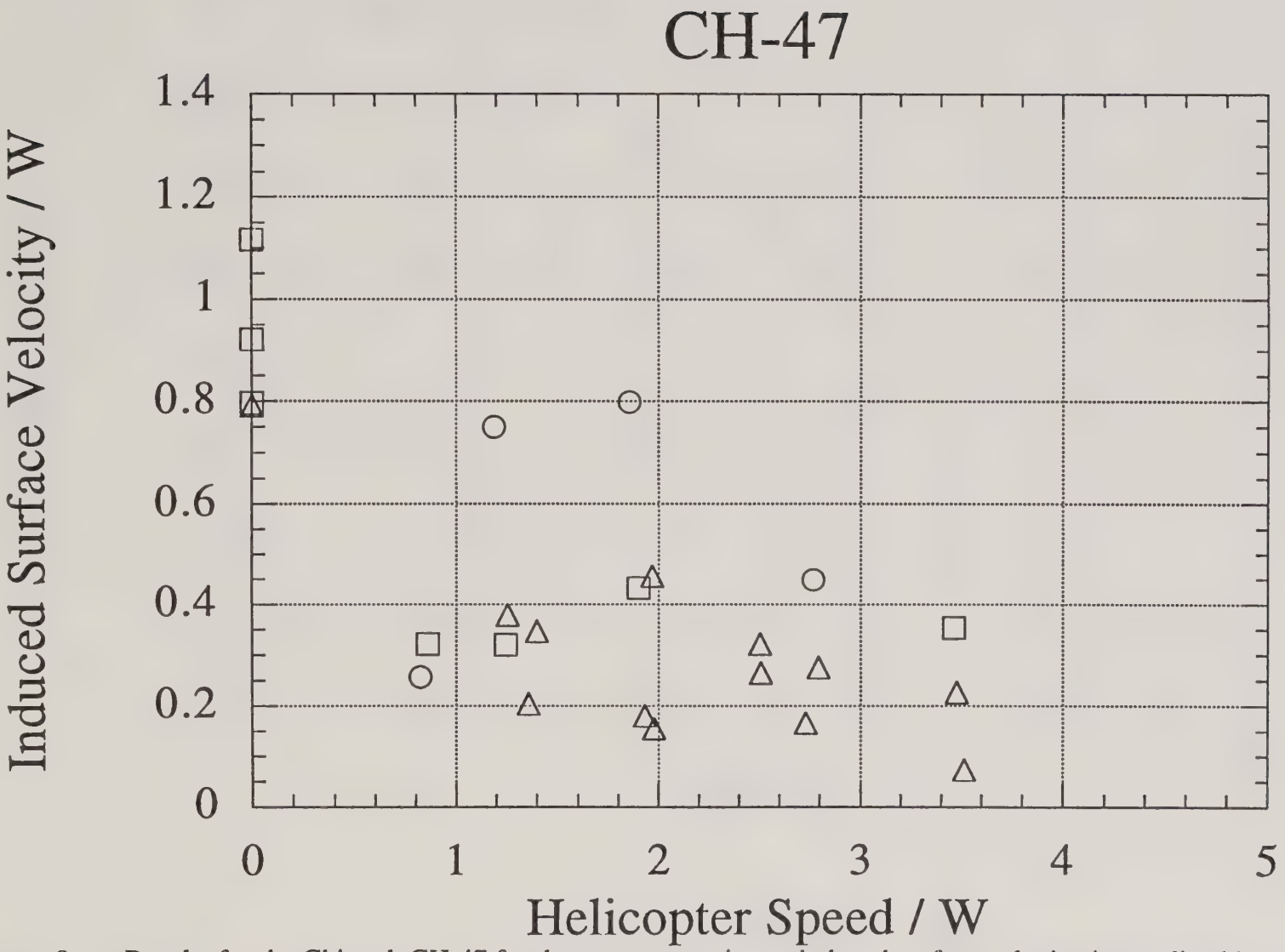

Figure 9a. Results for the Chinook CH-47 for the average maximum induced surface velocity (normalized by the downwash speed W) plotted as a function of helicopter speed over the tower grid (also normalized by W) for 24 trial runs. Here the nominal helicopter heights are identified: less than 60 m (open circles), 60 m to 80 m (open squares) and greater than 80 m (open triangles).

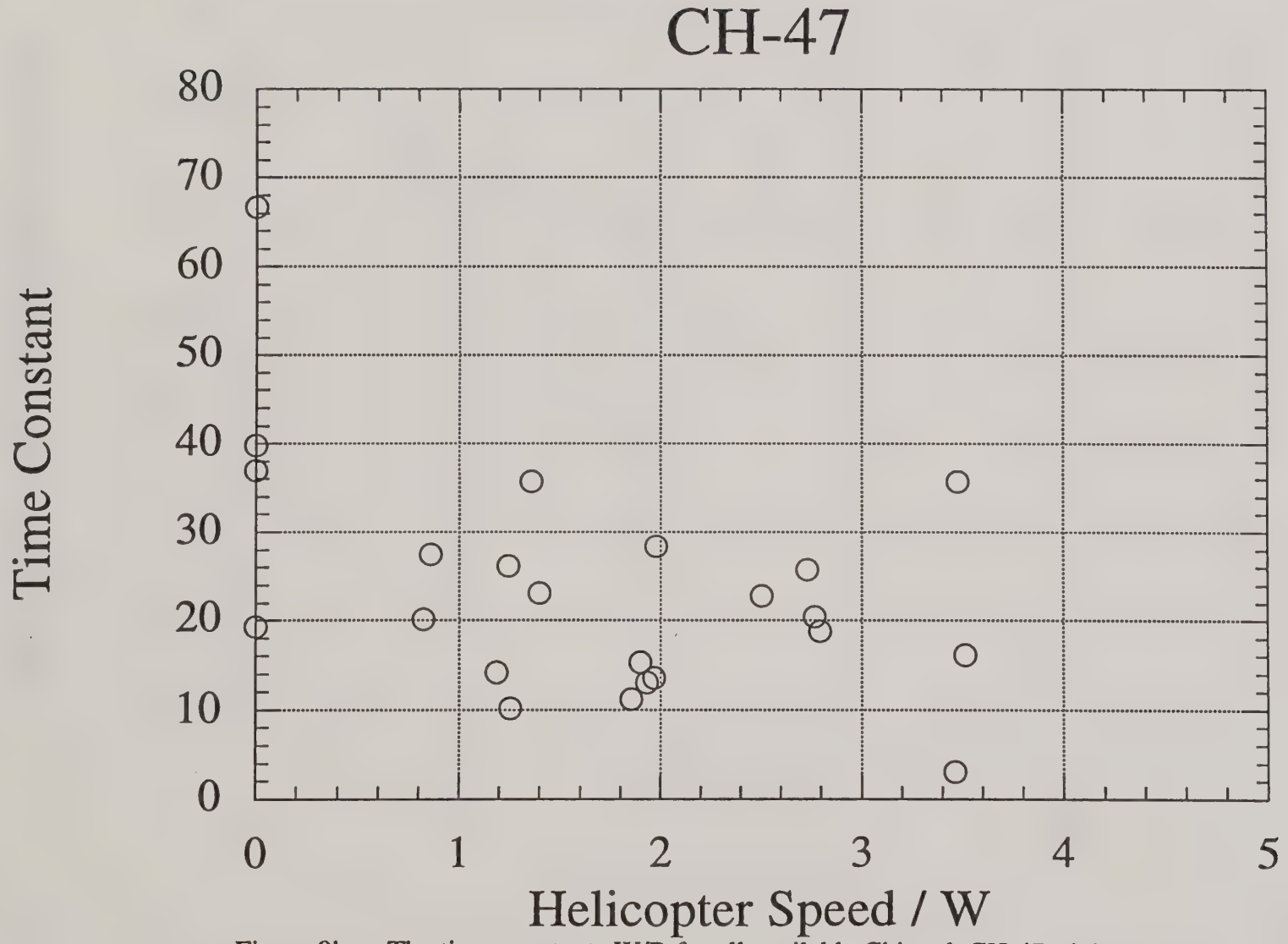

Figure 9b. The time constant τW/R for all available Chinook CH-47 trial runs.

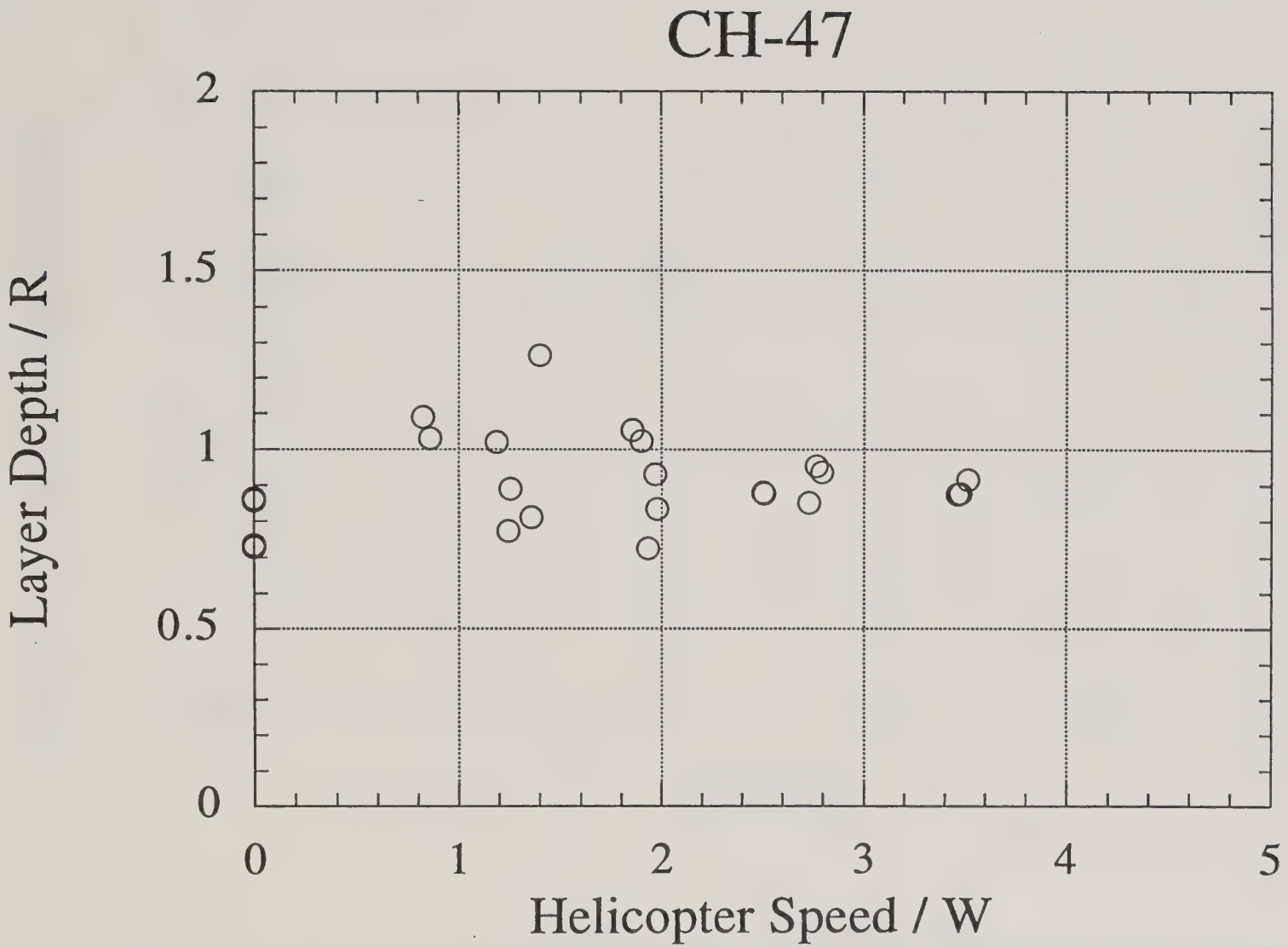

Figure 9c. The average layer depth normalized by the rotor radius R for the Chinook CH-47 trial runs.

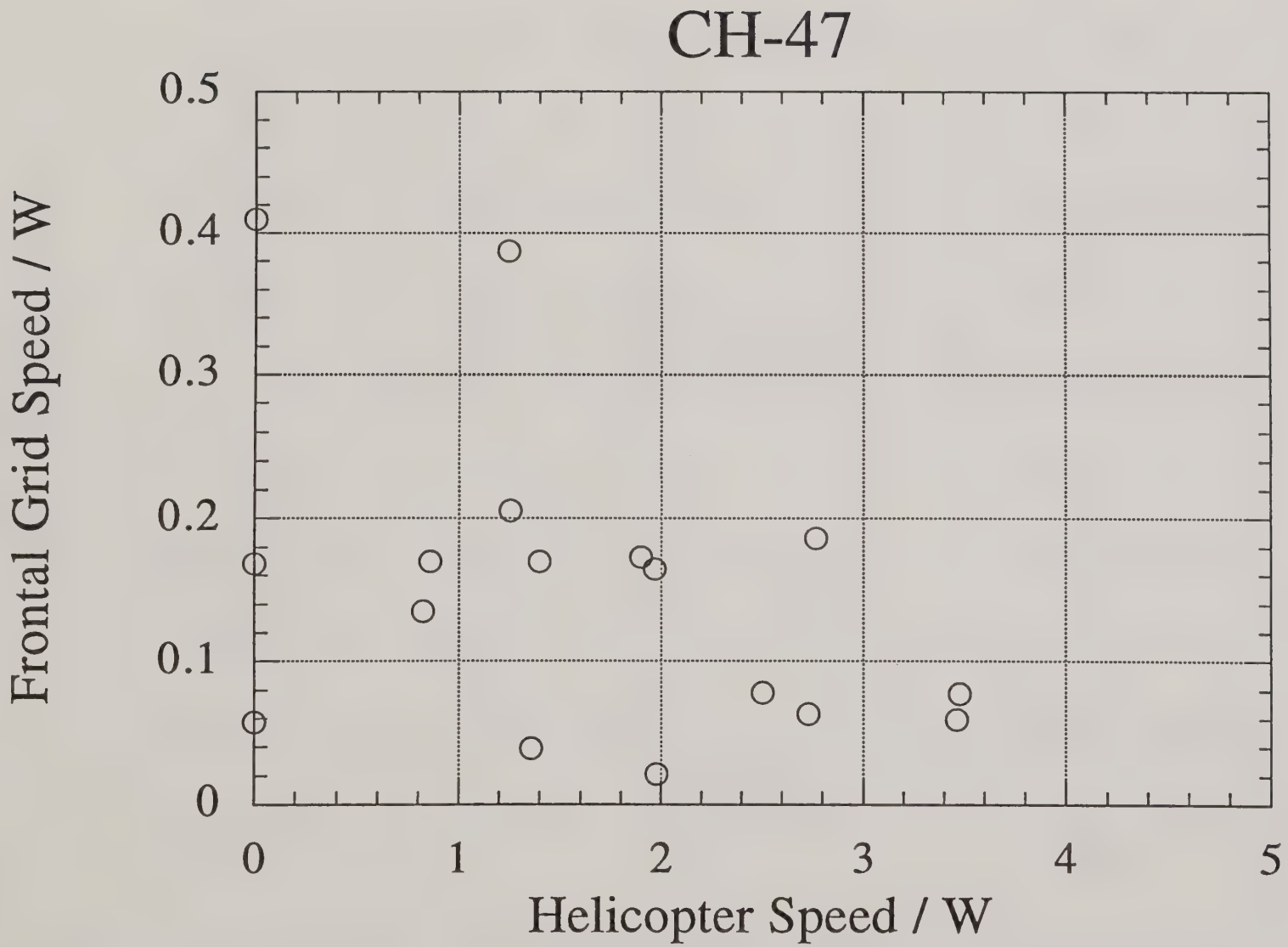

Figure 9d. The average frontal grid speed normalized by the downwash speed W for the Chinook CH-47 trial runs.

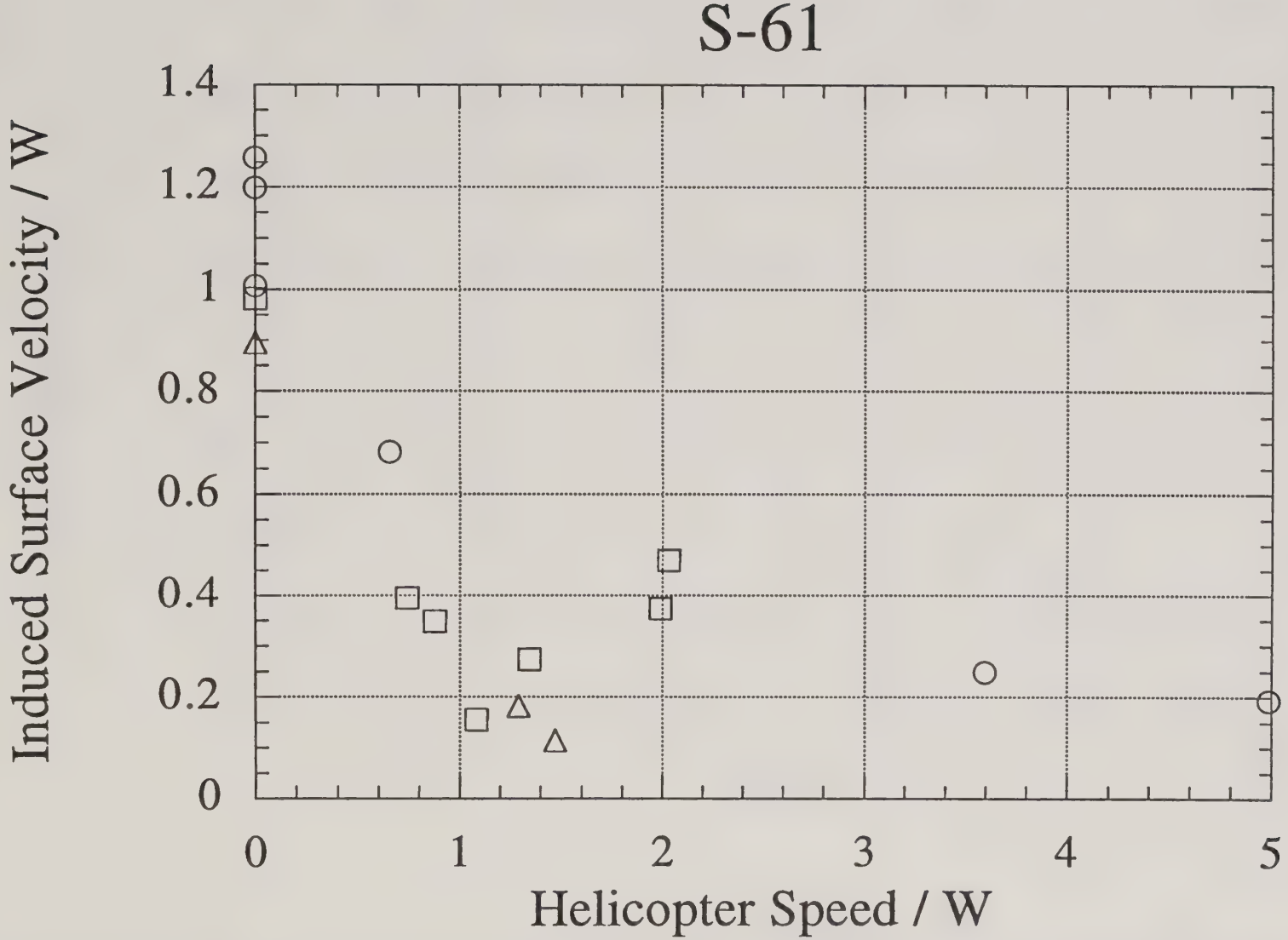

Figure 10a. Results for the Sikorsky S-61 for the average maximum induced surface velocity (normalized by the downwash speed W) plotted as a function of helicopter speed over the tower grid (also normalized by W) for 16 trial runs. Here the nominal helicopter heights are identified: less than 60 m (open circles), 60 m to 80 m (open squares) and greater than 80 m (open triangles).

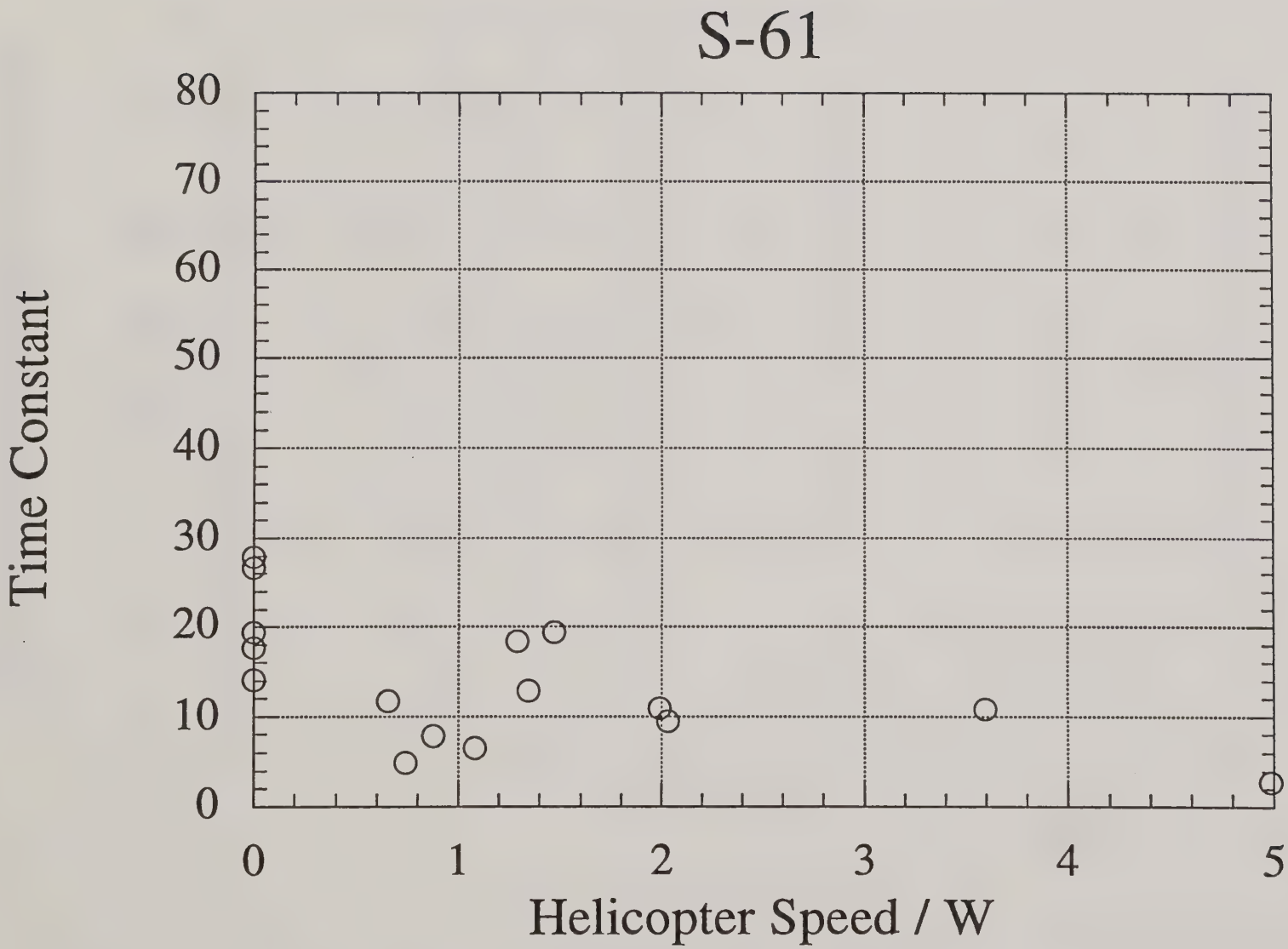

Figure 10b. The time constant τW/R for all available Sikorsky S-61 trial runs.

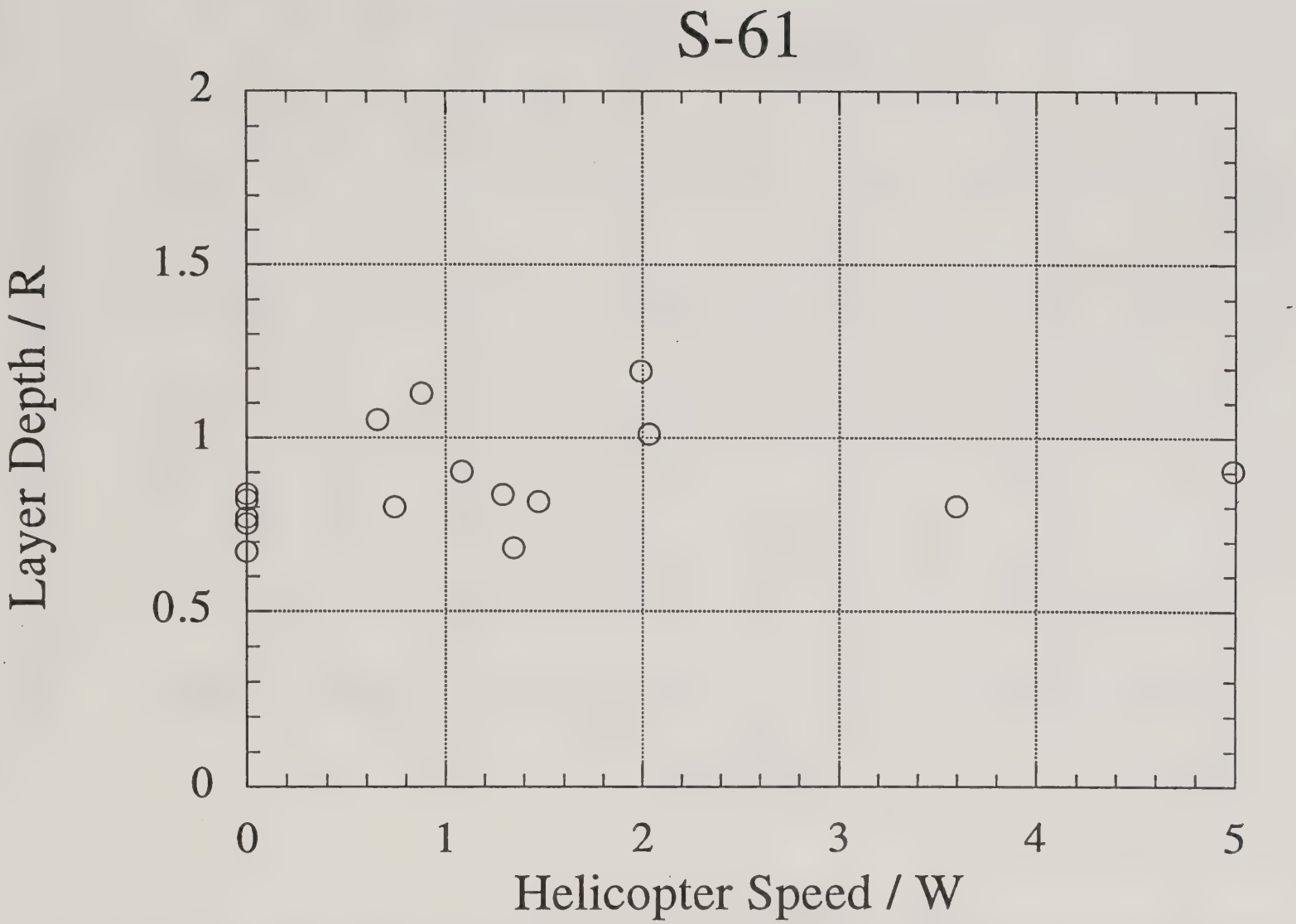

Figure 10c. The average layer depth normalized by the rotor radius R for the Sikorsky S-61H trial runs.

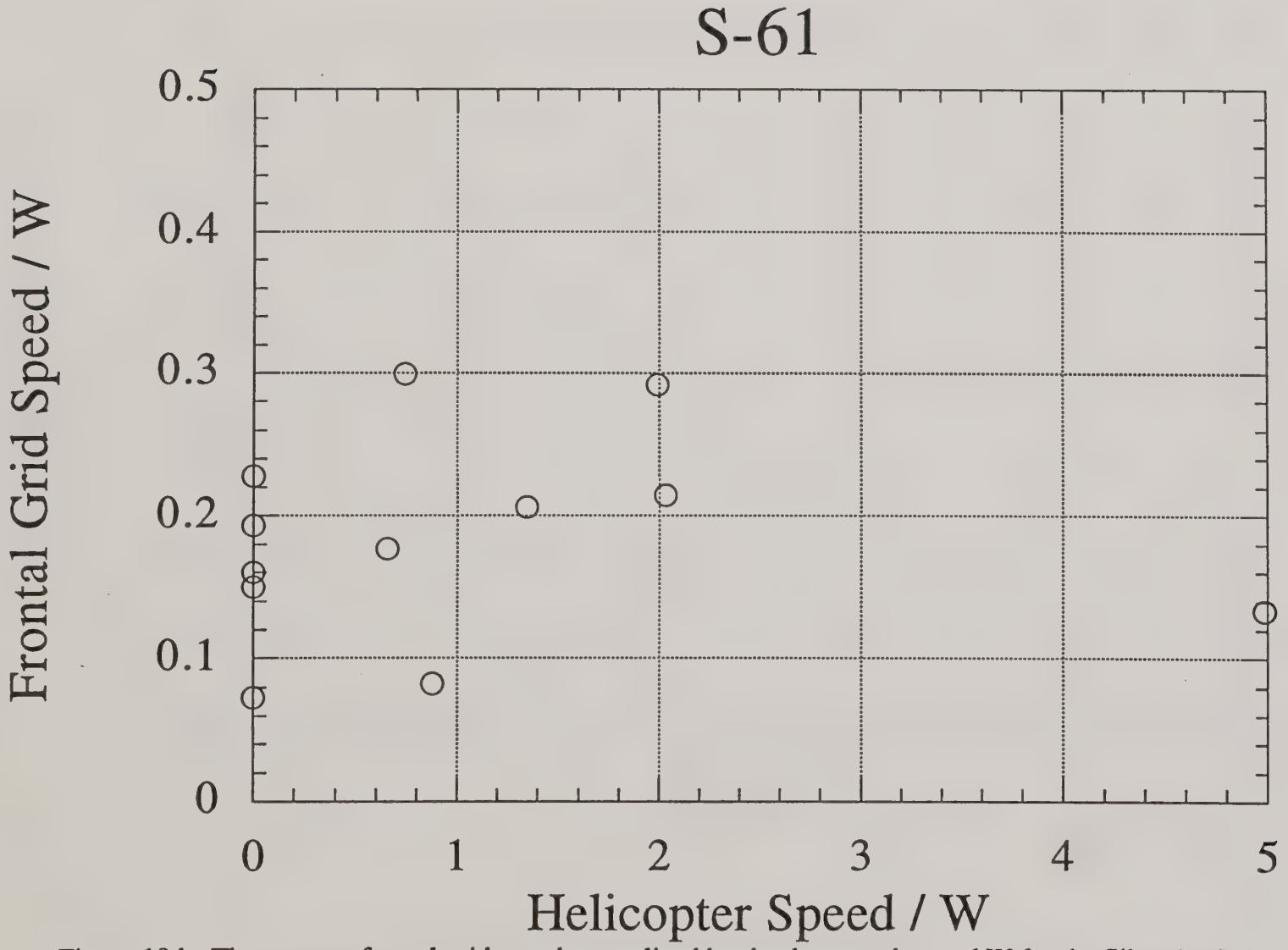

Figure 10d. The average frontal grid speed normalized by the downwash speed W for the Sikorsky S-61 trial runs.

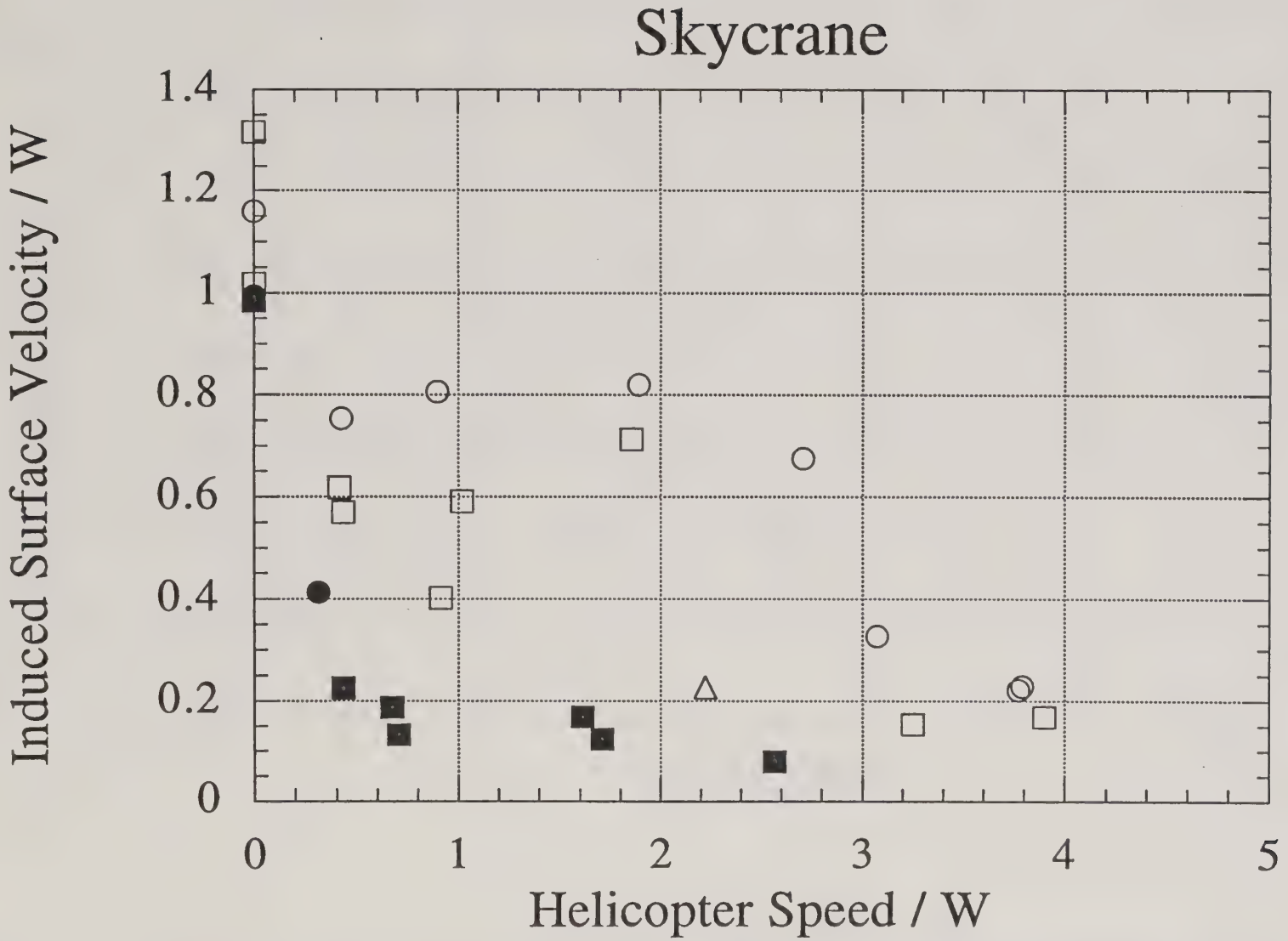

Figure 11a. Results for the Skycrane for the average maximum induced surface velocity (normalized by the downwash speed W) plotted as a function of helicopter speed over the tower grid (also normalized by W) for 27 trial runs. Here the nominal helicopter heights are identified: less than 40 m (open circles), 40 m to 60 m (open squares), 60 m to 80 m (open triangles), 80 m to 100 m (closed circles) and greater than 100 m (closed squares).

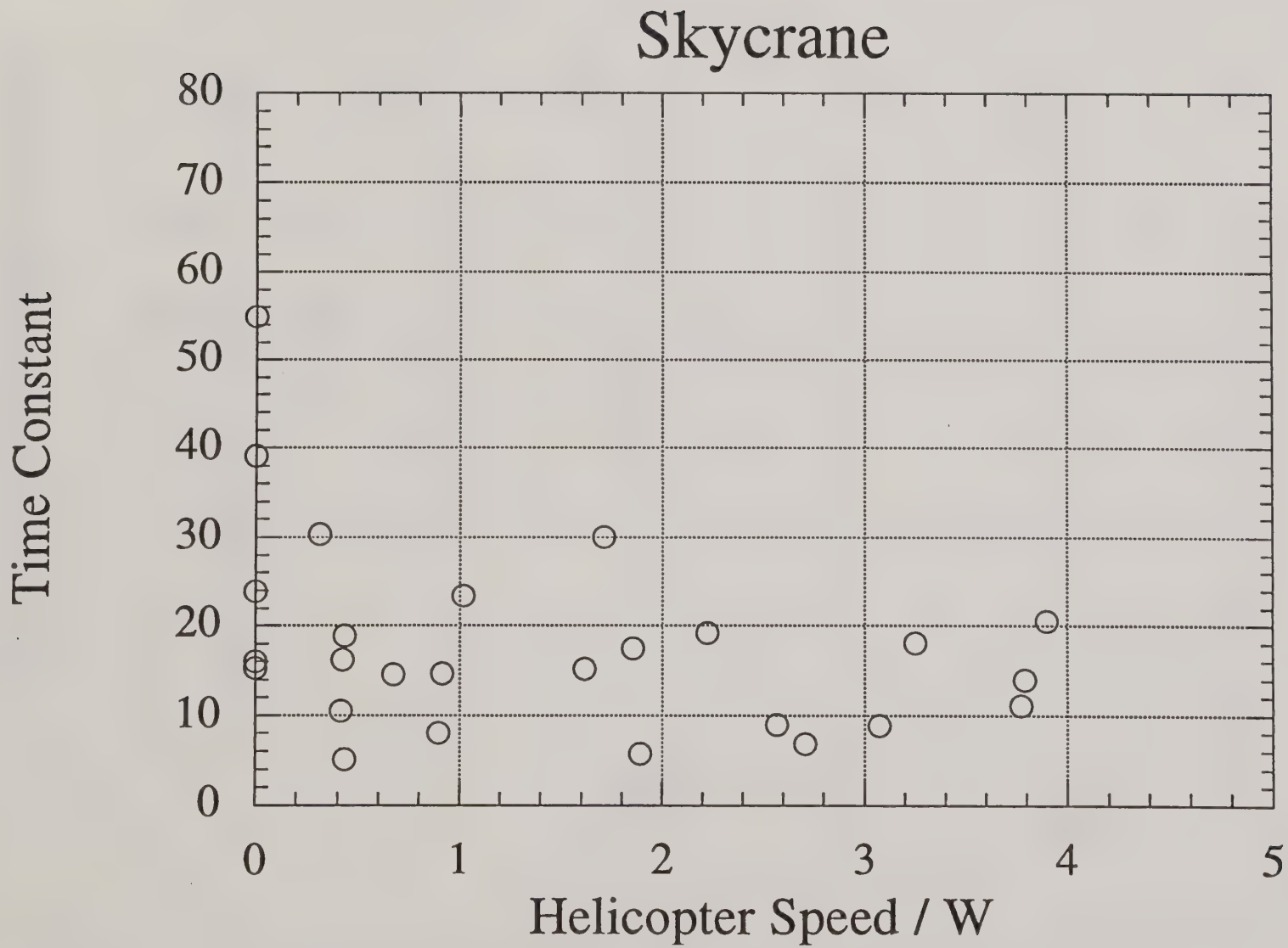

Figure 11b. The time constant τW/R for all available Skycrane trial runs.

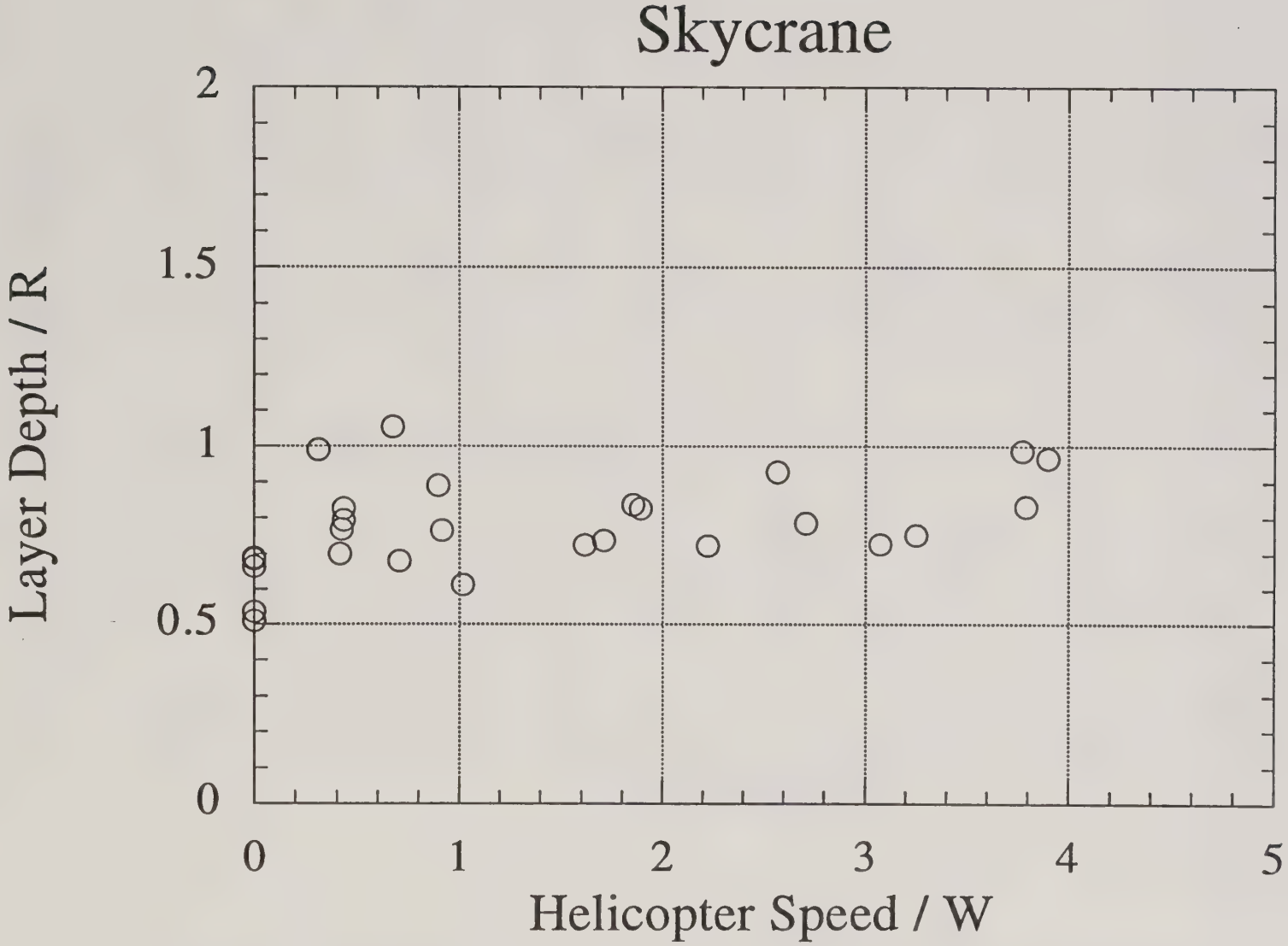

Figure 11c. The average layer depth normalized by the rotor radius R for the Skycrane trial runs.

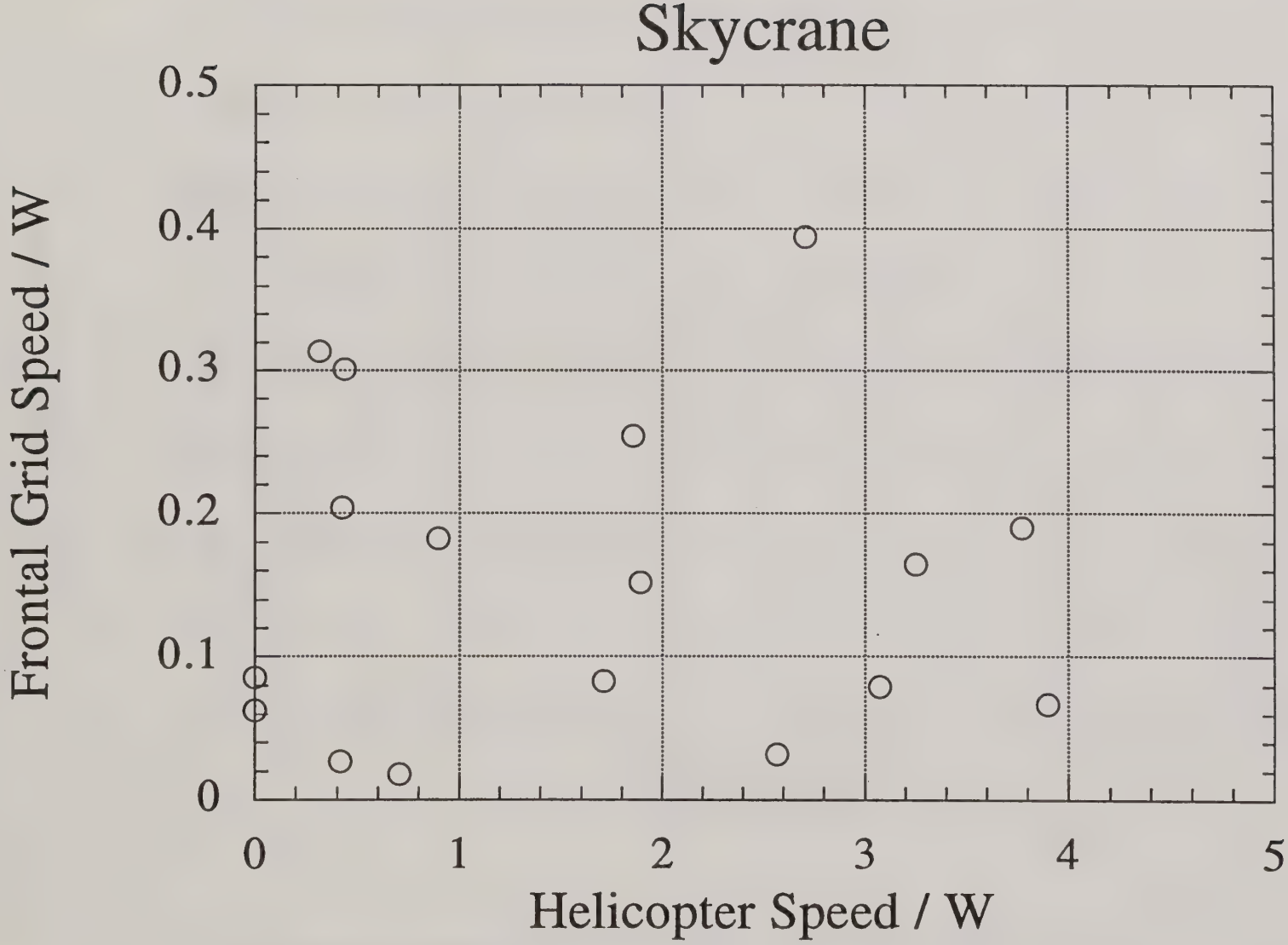

Figure 11d. The average frontal grid speed normalized by the downwash speed W for the Skycrane trial runs.

4. CONCLUSIONS

A field study in Yuba City, CA has resulted in 181 field runs of helicopters at various speeds and heights passing over an anemometer tower grid. Data reduction and interpretation suggest that the induced surface velocities and gust front depth are consistent with idealized models of the phenomenon. The new results -- the decay of the maximum winds and the outward speed of the resulting gust fronts -- should be of value when evaluating the influence of the passing helicopter on the dispersal of fire, pesticides, dusts, aerosols, or other contaminants.

5. ACKNOWLEDGMENTS

This cooperative study was sponsored by the USDA Forest Service, State and Private Forestry, Forest Pest Management; USDA Forest Service, Intermountain Research Station, Fire Laboratory; and the U. S. Army. We would like to acknowledge the assistance of Chuck George and Greg Johnson (USDA Forest Service, Intermountain Research Station) and Bruce Grim (U. S. Army) for enabling this research effort.

6. REFERENCES

Bilanin, A. J., M. E. Teske, J. W. Barry and R. B. Ekblad. 1989a. Project WIND Anemometer Tower Flyby Data Reduction. Proceedings of the 19th Conference on Agricultural and Forest Meteorology. American Meteorological Society: Charleston, SC. pp. 188-201.

Bilanin, A. J., M. E. Teske, J. W. Barry and R. B. Ekblad. 1989b. AGDISP: The Aircraft Spray Dispersion Model, Code Development and Experimental Validation. *Transactions of the American Society of Agricultural Engineers* 32(1): 327-334.

Teske, M. E. 1988. AGDISP Analysis of Vortex Decay from Program WIND Phases I and III. Technical Note No. 88-6. Continuum Dynamics, Inc.: Princeton, NJ.

Teske, M. E., A. J. Bilanin and J. W. Barry. 1993. Decay of Aircraft Vortices Near the Ground. *AIAA Journal* 31(8): 1531-1533.

Teske, M. E., A. J. Bilanin and R. G. Geyer. 1986. Field Study of Interaction of Spray Aircraft Wake with Convective Surface Winds in Hilly Terrain. Report No. 86-5. Continuum Dynamics, Inc.: Princeton, NJ.

Teske, M. E., J. F. Bowers, J. E. Rafferty and J. W. Barry. 1993. FSCBG: An Aerial Spray Dispersion Model for Predicting the Fate of Released Material Behind Aircraft. *Environmental Toxicology and Chemistry* 12(3): 453-464.

Teske, M. E., A. E. Kaufman and T. B. Curbishley. 1988. Dugway Tower Flyby Data Collection, Reduction and Interpretation. Technical Note No. 88-11. Continuum Dynamics, Inc.: Princeton, NJ.

Teske, M. E., A. E. Kaufman and T. B. Curbishley. 1990. Additional Dugway Tower Flyby Data Collection, Reduction and Interpretation. Technical Note No. 90-14. Continuum Dynamics, Inc.: Princeton, NJ.

Williamson, G. G., M. E. Teske and R. G. Geyer. 1985. Experimental Study of Aircraft Wakes in Forest Canopies. Report No. 85-7. Continuum Dynamics, Inc.: Princeton, NJ.

7. APPENDIX

For the convenience of the reader, the induced surface velocities generated by the seven helicopters in the field study (Bell 205H, Bell 206B, Blackhawk, Boeing Vertol BV-107, Chinook CH-47, Sikorsky S-61, and Skycrane) are plotted here in dimensional units.

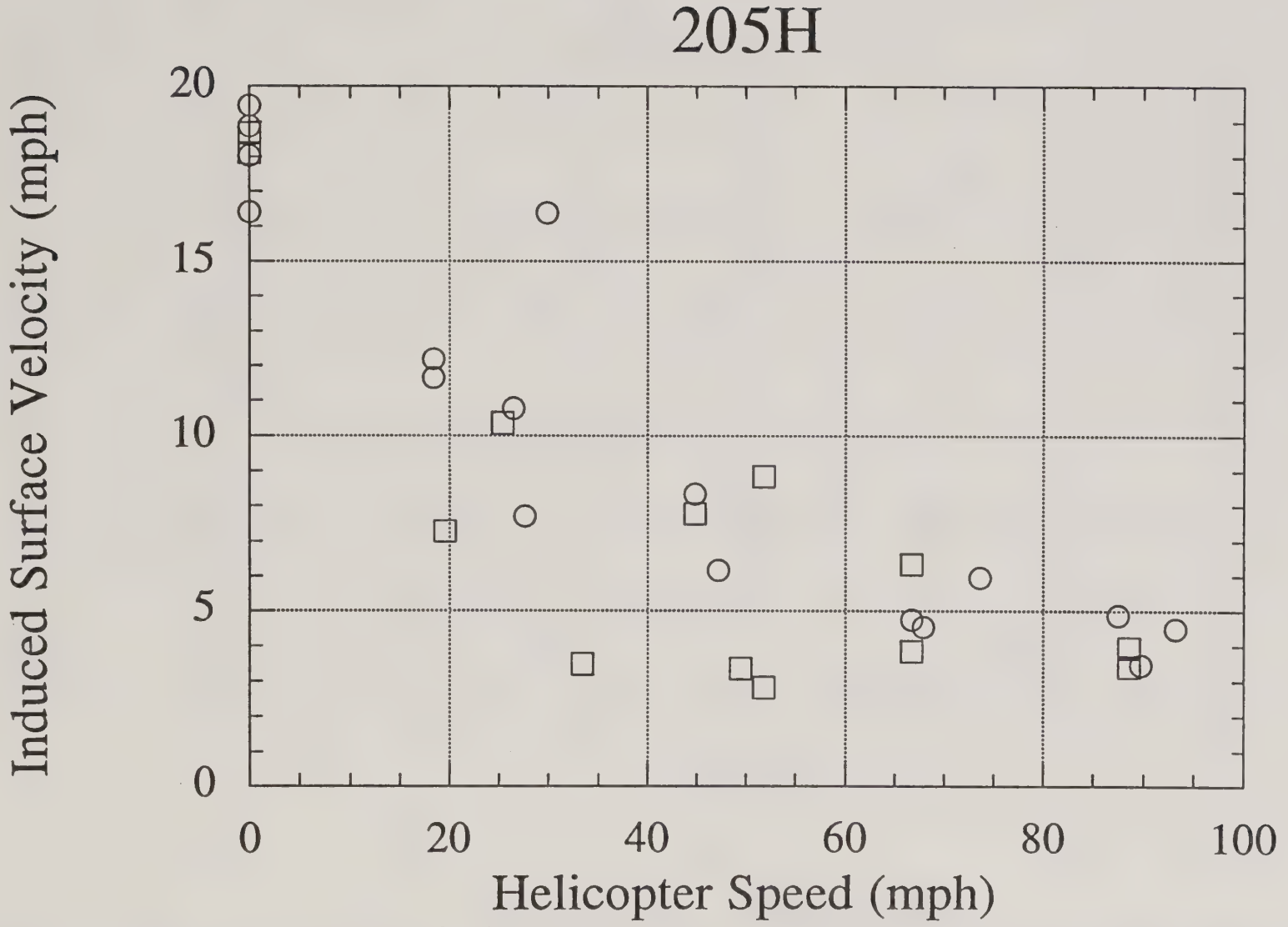

Figure A1. Results for the Bell 205H for the average maximum induced surface velocity (in miles per hour) plotted as a function of helicopter speed over the tower grid (also in miles per hour) for 30 trial runs. Here the nominal helicopter heights are identified: less than 100 feet (open circles) and greater than 100 feet (open squares).

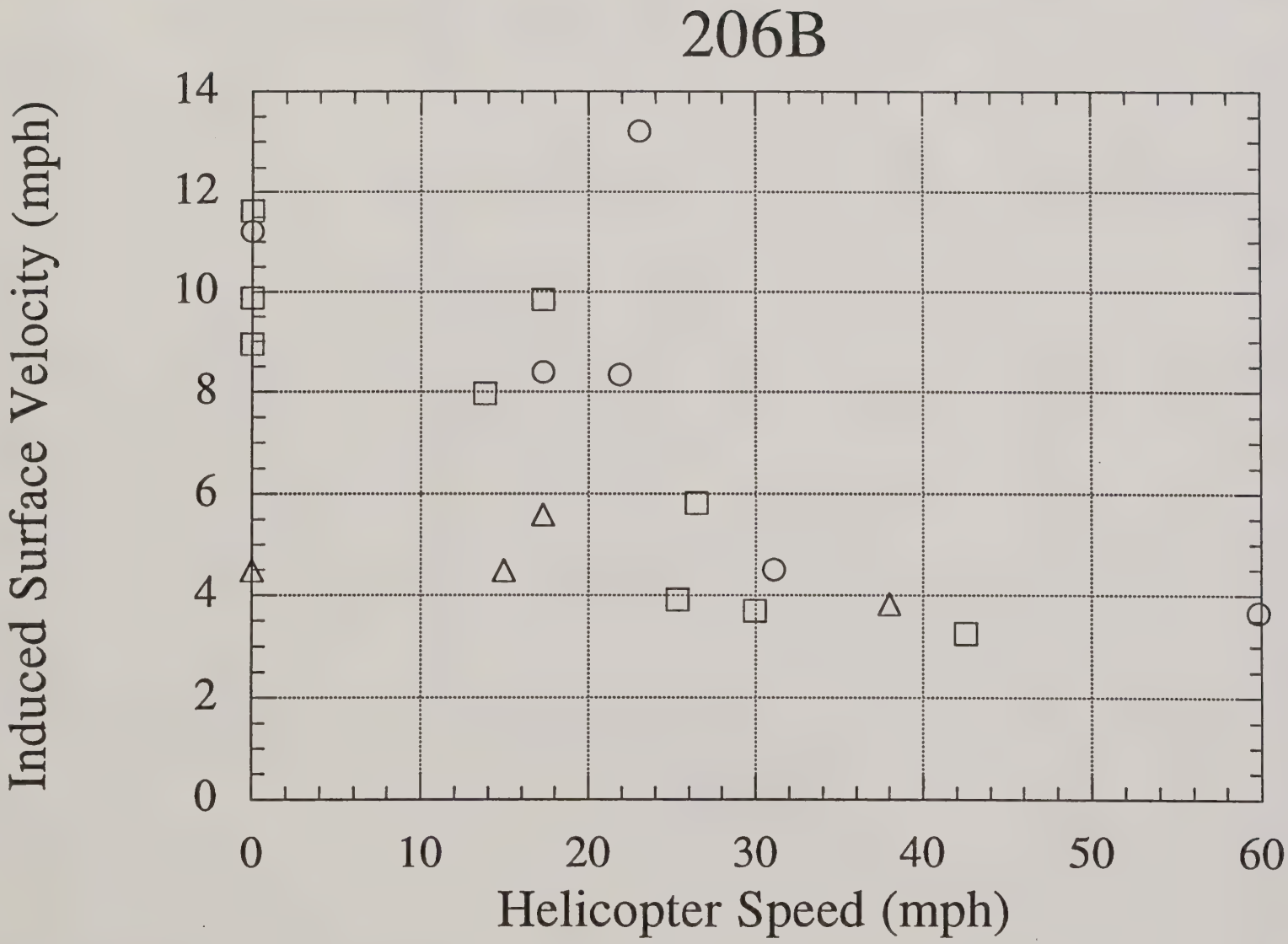

Figure A2. Results for the Bell 206B for the average maximum induced surface velocity (in miles per hour) plotted as a function of helicopter speed over the tower grid (also in miles per hour) for 19 trial runs. Here the nominal helicopter heights are identified: less than 100 feet (open circles), 100 feet to 130 feet (open squares) and greater than 130 feet (open triangles).

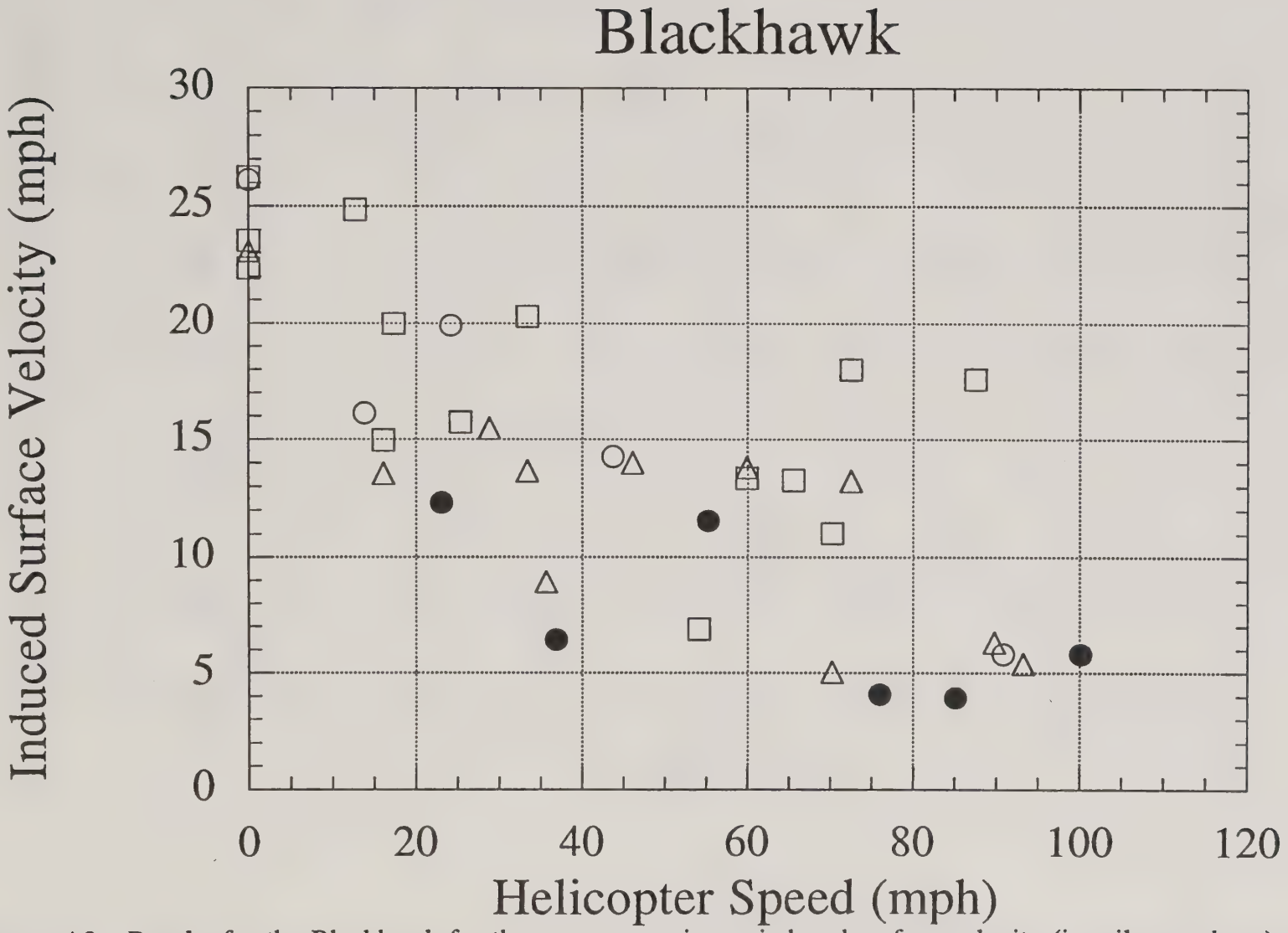

Figure A3. Results for the Blackhawk for the average maximum induced surface velocity (in miles per hour) plotted as a function of helicopter speed over the tower grid (also in miles per hour) for 36 trial runs. Here the nominal helicopter heights are identified: less than 100 feet (open circles), 100 feet to 130 feet (open squares), 130 feet to 195 feet (open triangles) and greater than 195 feet (closed circles).

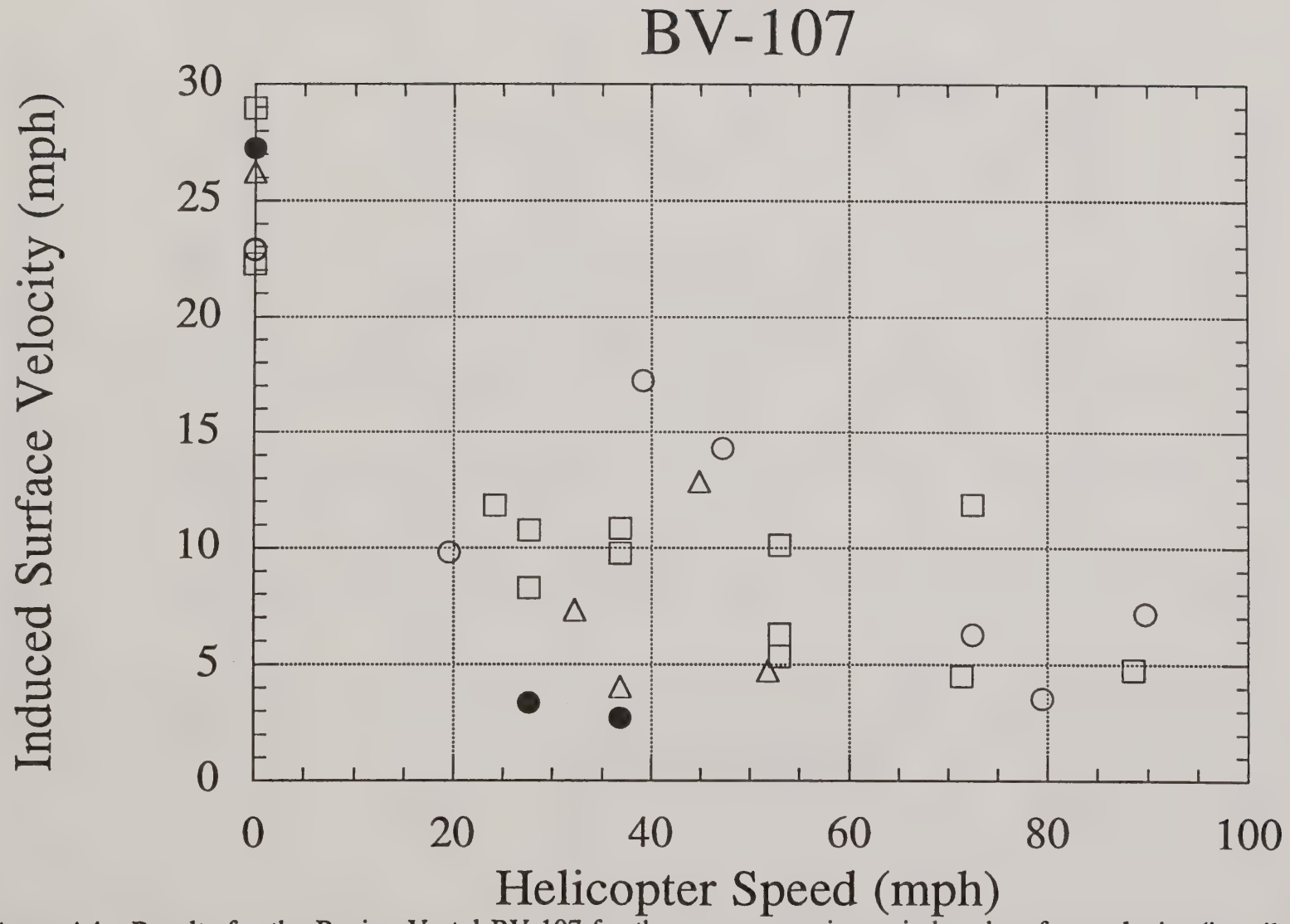

Figure A4. Results for the Boeing Vertol BV-107 for the average maximum induced surface velocity (in miles per hour) plotted as a function of helicopter speed over the tower grid (also in miles per hour) for 29 trial runs. Here the nominal helicopter heights are identified: less than 130 feet (open circles), 130 feet to 195 feet (open squares), 195 feet to 260 feet (open triangles) and greater than 260 feet (closed circles).

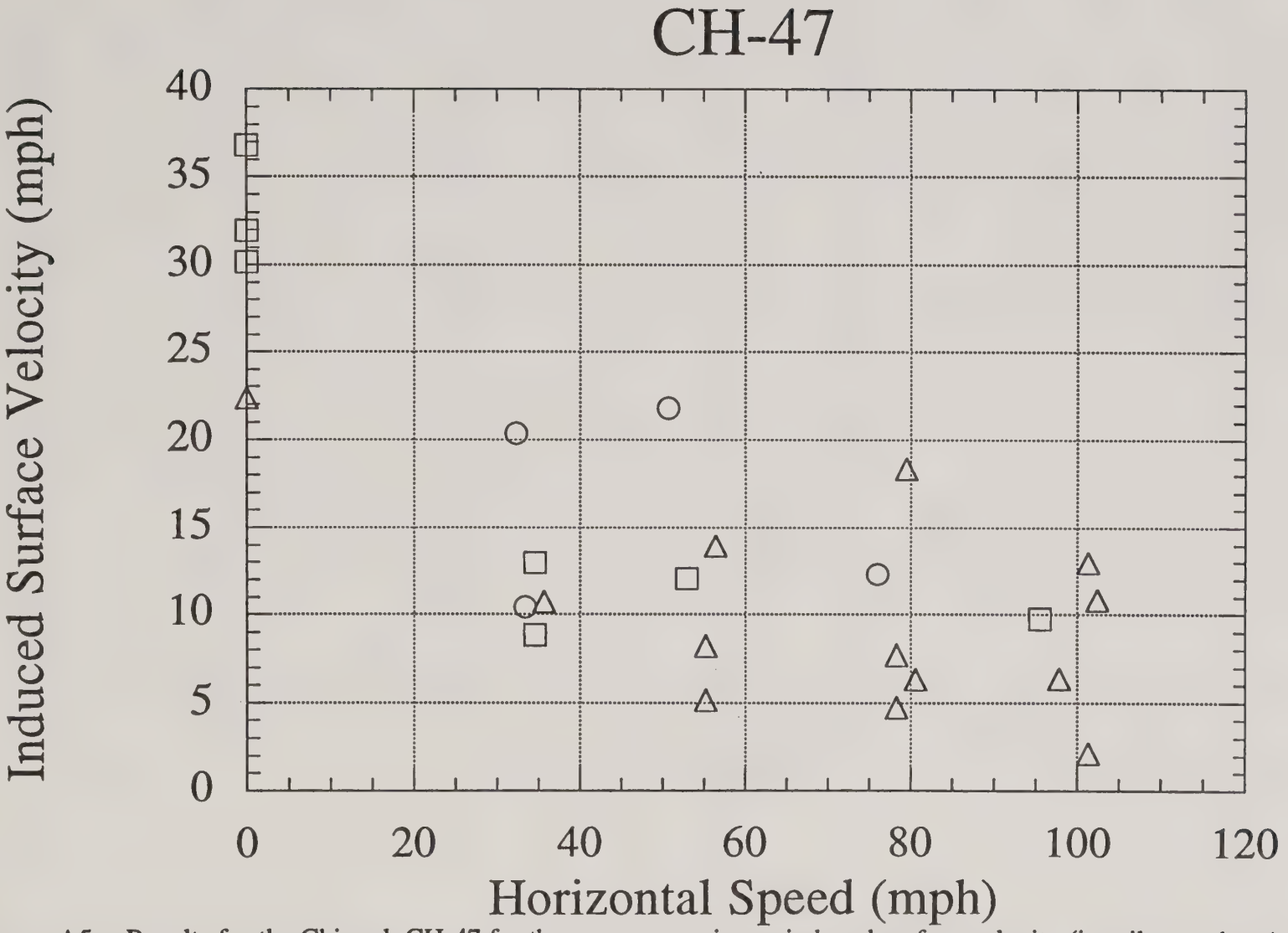

Figure A5. Results for the Chinook CH-47 for the average maximum induced surface velocity (in miles per hour) plotted as a function of helicopter speed over the tower grid (also in miles per hour) for 24 trial runs. Here the nominal helicopter heights are identified: less than 195 feet (open circles), 195 feet to 260 feet (open squares) and greater than 260 feet (open triangles).

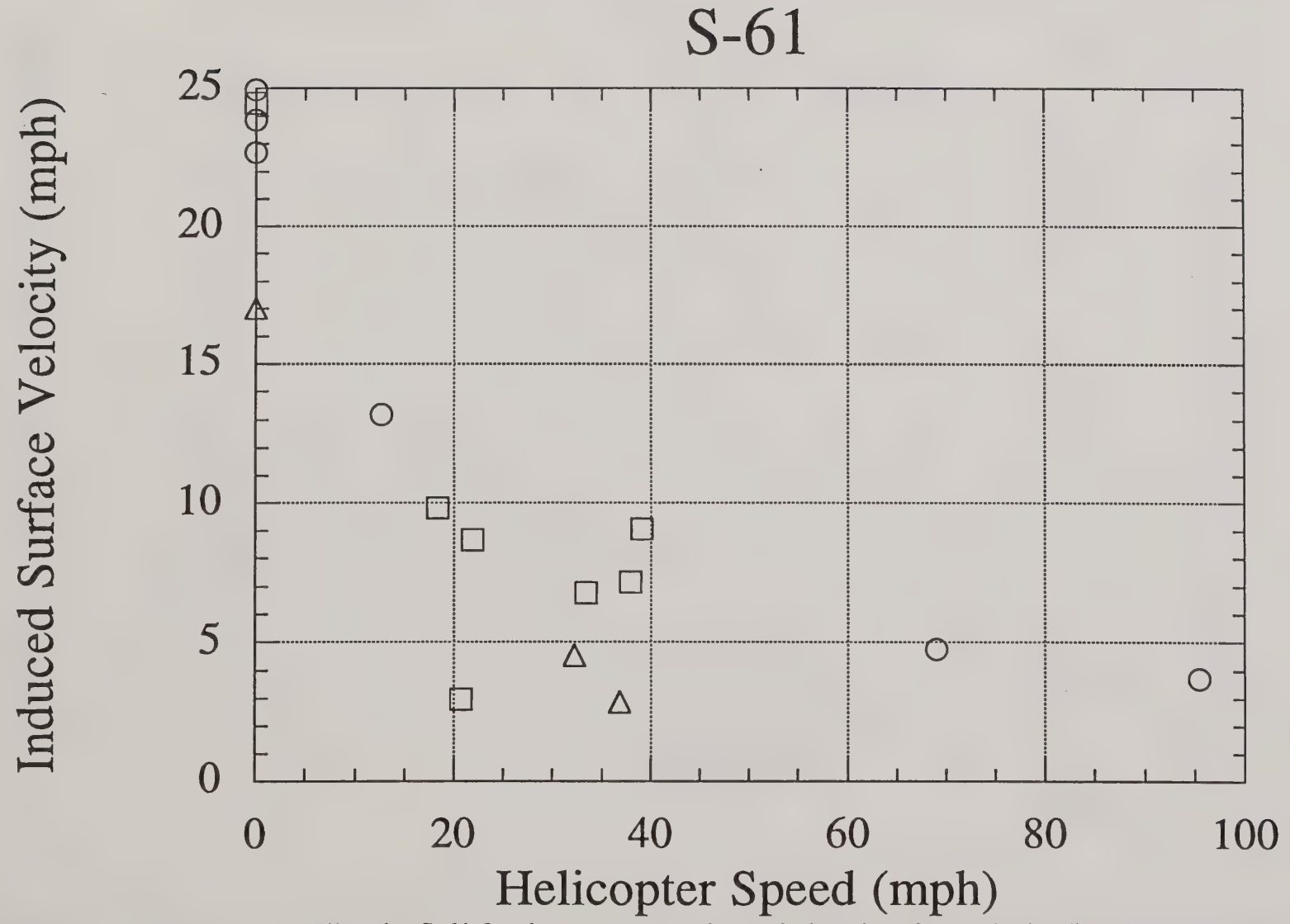

Figure A6. Results for the Sikorsky S-61 for the average maximum induced surface velocity (in miles per hour) plotted as a function of helicopter speed over the tower grid (also in miles per hour) for 16 trial runs. Here the nominal helicopter heights are identified: less than 195 feet (open circles), 195 feet to 260 feet (open squares) and greater than 260 feet (open triangles).

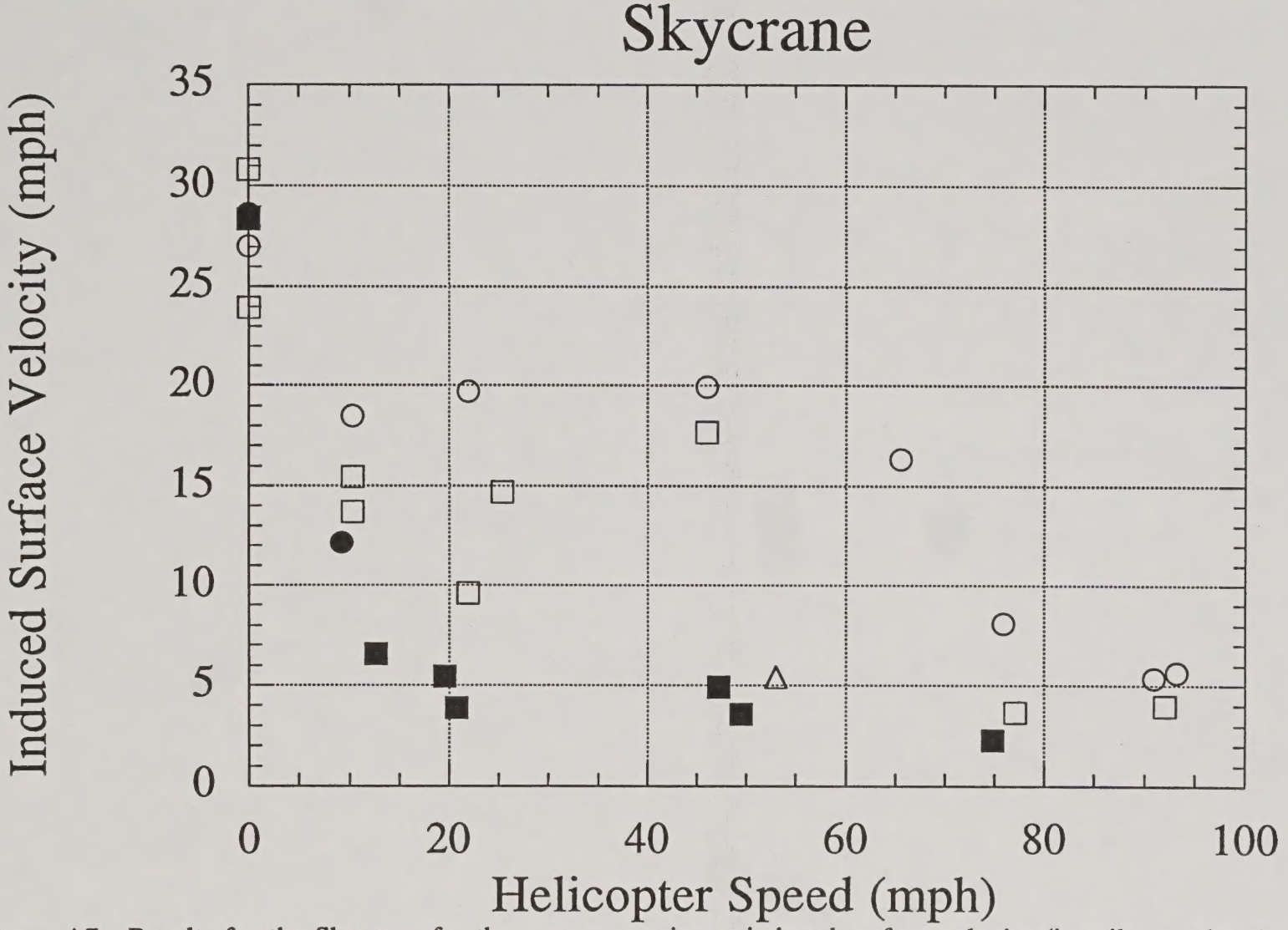

Figure A7. Results for the Skycrane for the average maximum induced surface velocity (in miles per hour) plotted as a function of helicopter speed over the tower grid (also in miles per hour) for 27 trial runs. Here the nominal helicopter heights are identified: less than 130 feet (open circles), 130 feet to 195 feet (open squares), 195 feet to 260 feet (open triangles), 260 feet to 330 feet (closed circles) and greater than 330 feet (closed squares).